OXFORD ACADEMIC

Monthly Notices of the Royal Astronomical Society

Royal Astronomical Society

Article Navigation

Hunting extreme BL Lacertae blazars with Fermi-Large Area Telescope

Get access >

M Nievas Rosillo, A Domínguez, G Chiaro, G La Mura, A Brill, V S Paliya

Monthly Notices of the Royal Astronomical Society, Volume 512, Issue 1, May 2022, Pages 137–159,
https://doi.org/10.1093/mnras/stac491
Published: 23 February 2022 **Article history** ▾

Cite Permissions Share ▾

ABSTRACT

The emission of very-high-energy (VHE) photons (E > 100 GeV) in blazars is closely connected to the production of ultra-relativistic particles and the role of these γ-ray sources as cosmic particle accelerators. This work focuses on a selection of 22 γ-ray objects from the 2BIGB catalogue of high-synchrotron-peaked

Instituto de Astrofísica de Canarias · IAC
Fermi Gamma-ray Space Telescope
γ 2022
7th Heidelberg International Symposium on **High Energy Gamma-Ray Astronomy**
Barcelona, July 4-8 2022

A multi-wavelength view of gamma-ray emitting extreme BL Lacertae blazar candidates hidden within Fermi-LAT data.

Mireia Nievas Rosillo - IAC / ULL Spain
Alberto Dominguez - UC Madrid, Spain
Graziano Chiaro - IASF / INAF Milano Italy
Giovanni La Mura - LIP Portugal
Ari Brill - Goddard / MD
Vaidehi S. Paliya - ARIES / India.

on behalf of the Fermi-LAT collaboration

email: mnievas@iac.es

Motivation

Source: TeVCat (251 entries)

	BL Lacs						
as of 2022/06 (VHE egal sky)	*HSP (EHSP)*	*ISP*	*LSP*	*FSRQ*	*FRI*	*Other AGNs*	*Starburst*
Number	55 (~15)	10	2	9	4-7	4-6	2

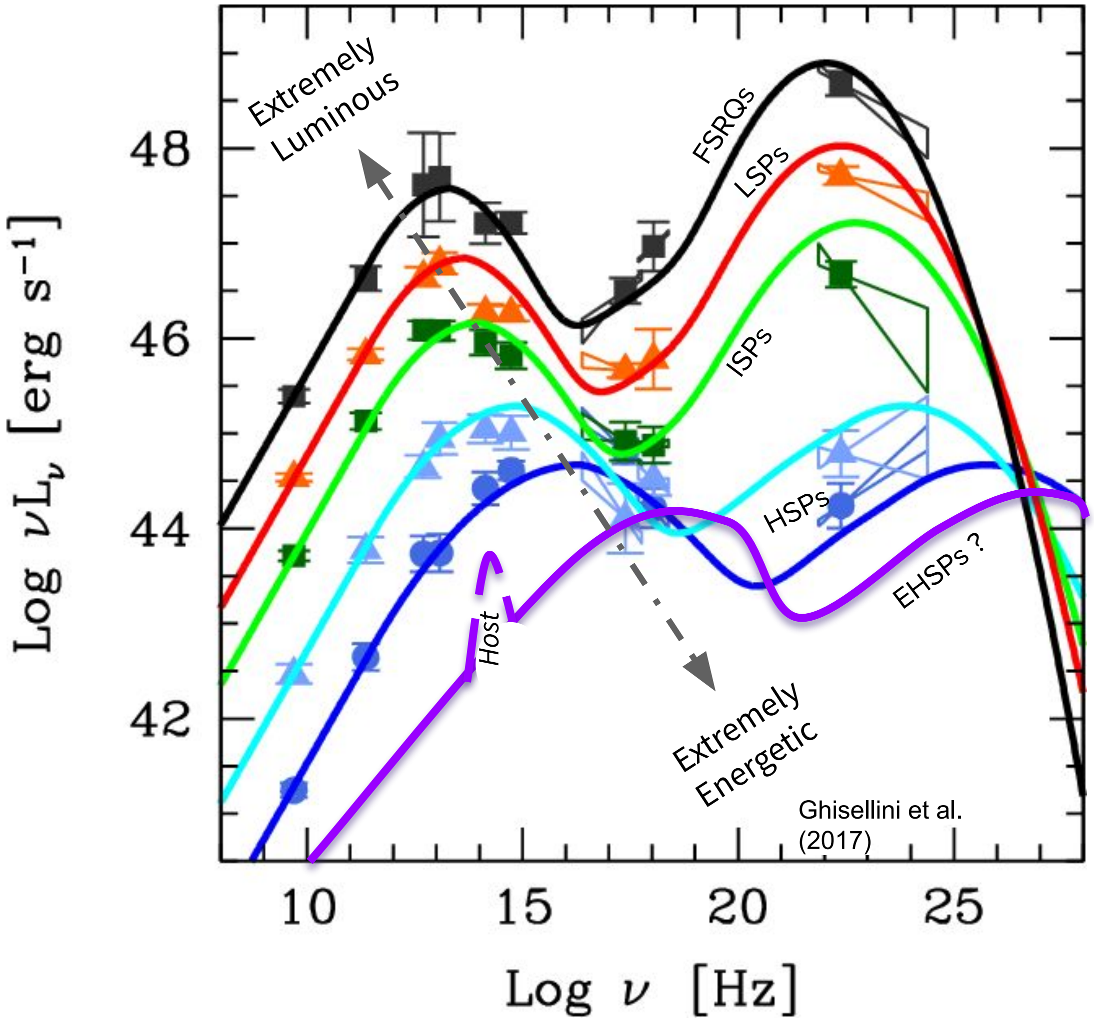

Blazar spectral classification

LSPs:
Synchrotron peak: < 10^{14} Hz

ISPs:
Synchrotron peak: 10^{14} to 10^{15} Hz

HSPs:
Synchrotron peak: 10^{15} to 10^{17} Hz

EHSPs:
Weak AGN emission, inefficient accretion, no optical emission lines, synchrotron spectra peaking at > 10^{17} Hz.
IC peak > 10^{26} Hz [?]

- *Difficult to detect (weak, hard spectrum)*
- *Host galaxy often visible*
- *Blazar sequence under review … biases?*
- *Transitional EHSPs vs classical EHSPs*

Classical EHSPs: HESS J1943+213

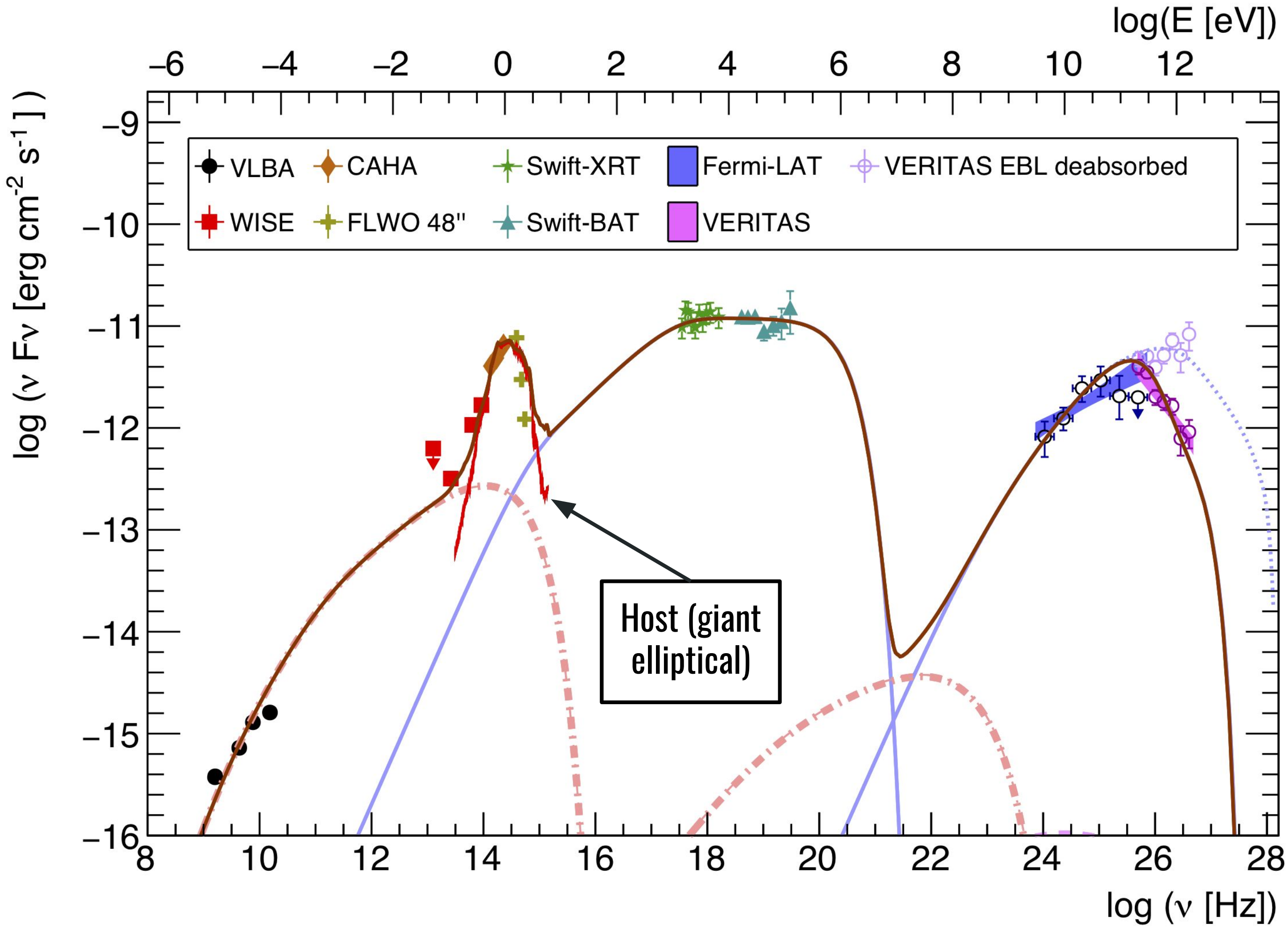

SED of HESS J1943+213, including the SSC model with components for a blob of relativistic particles (solid light blue curves) and a larger conical jet (dash-dotted red curves). **VERITAS, ApJ 862: 41, 2018.**

Redshift: 0.03 < z < 0.23 from host gal. size/photometry [Peter et al. 2014] + Fermi to VHE extrapolations [VERITAS ApJ 862: 41, 2018]

Transitional EHSPs

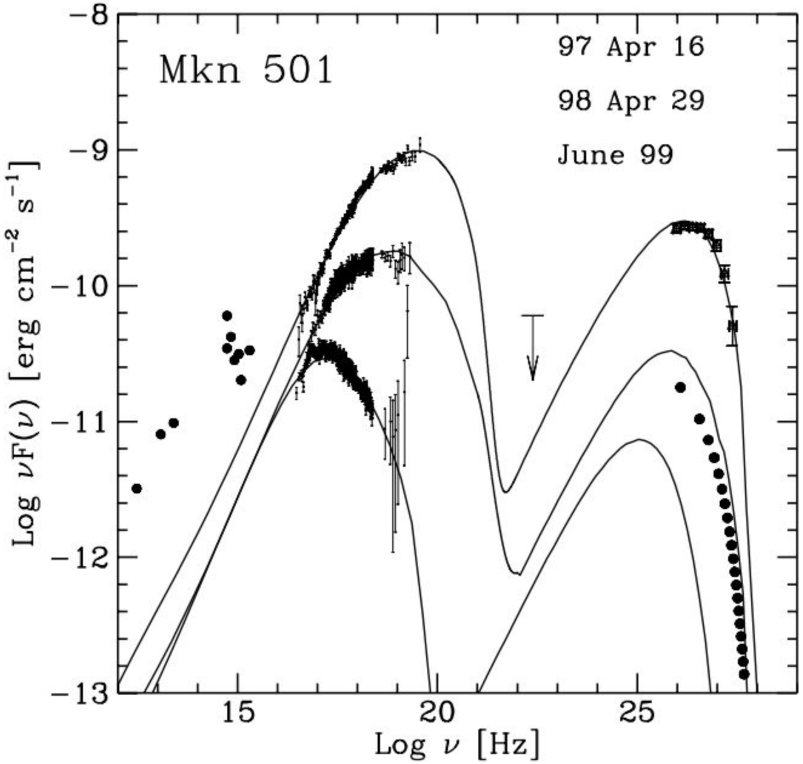

Mrk 501:
Tavecchio et al. 2001 ApJ 554:725-733

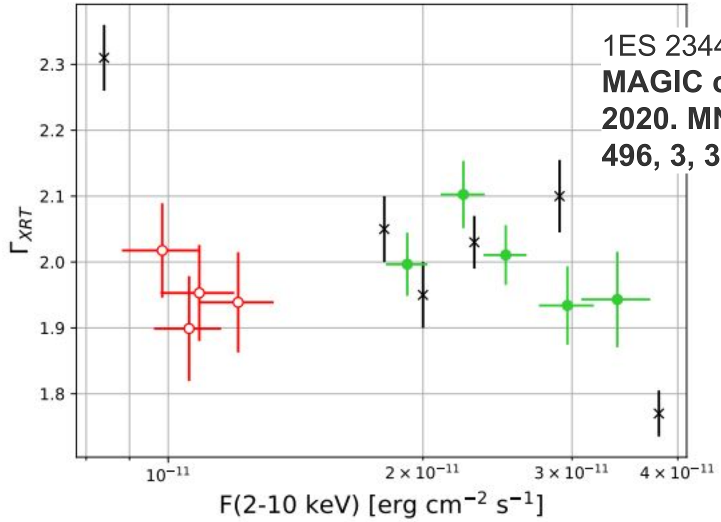

1ES 2344+514:
MAGIC coll. 2020. MNRAS 496, 3, 3912-3928

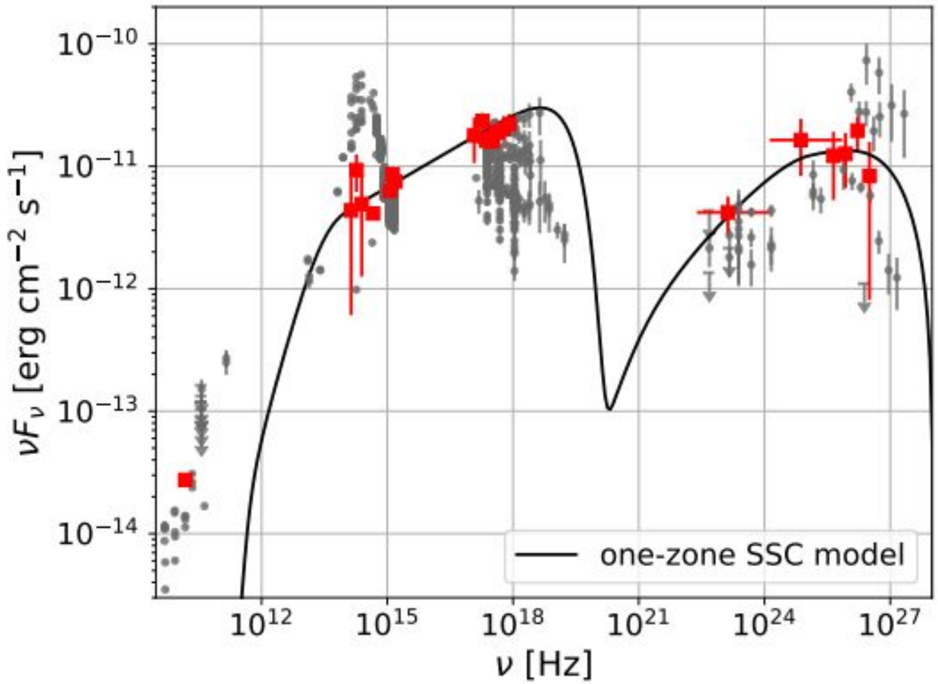

VHE-loud EHSPs

Foffano et al. 2019. MNRAS 486, 2, 1741-1762

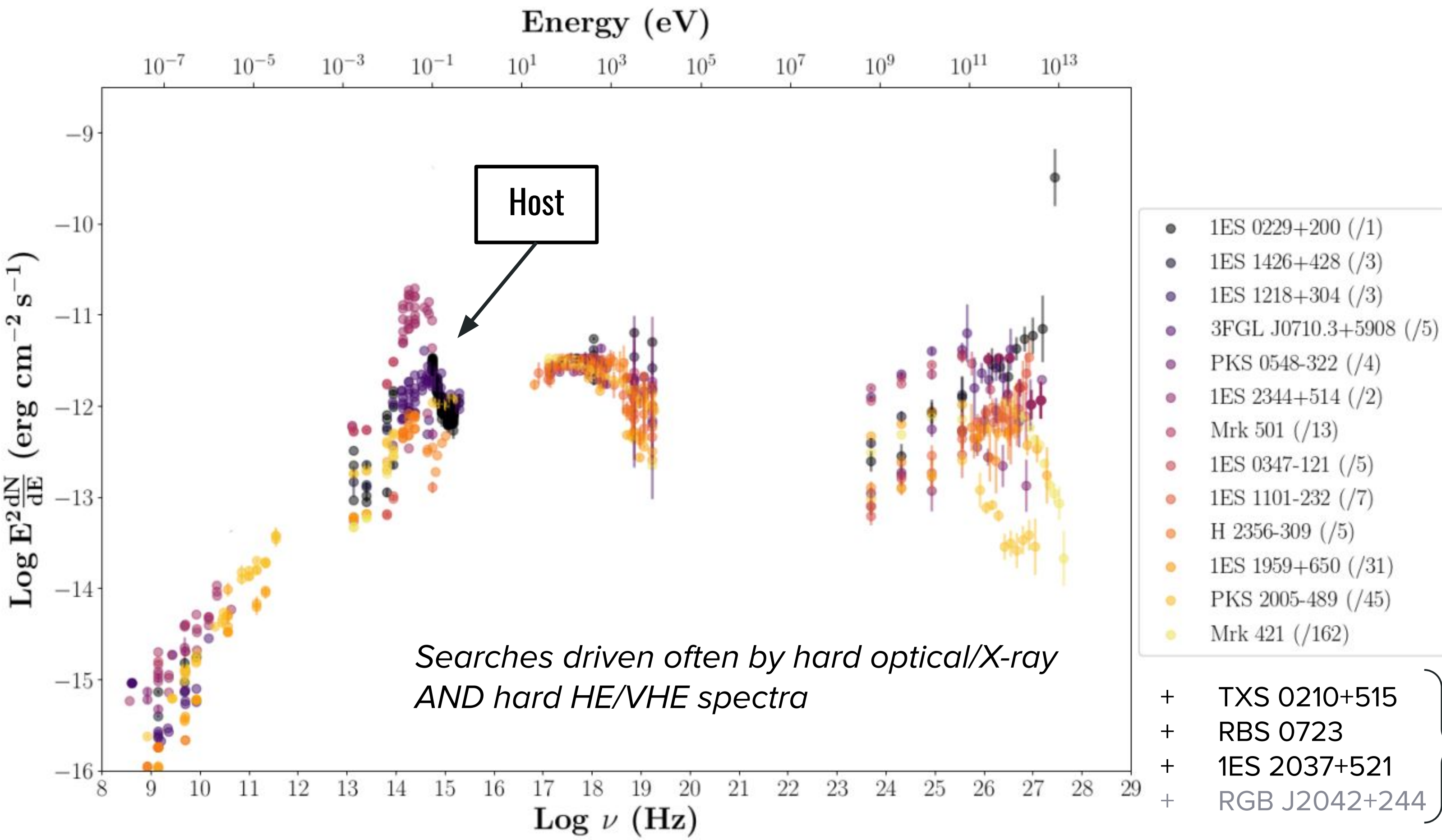

MAGIC 2020, ApJS 247, 1, 16

(a) Superimposition of the MWL SEDs of the 13 already TeV gamma-ray detected sources with publicly available TeV data. The fluxes have been rescaled to the 1ES 0229+200 flux of $3.34 \cdot 10^{-12}$ erg cm^{-2} s^{-1} at $1.7 \cdot 10^{17}$ Hz.

Methodology

Source selection

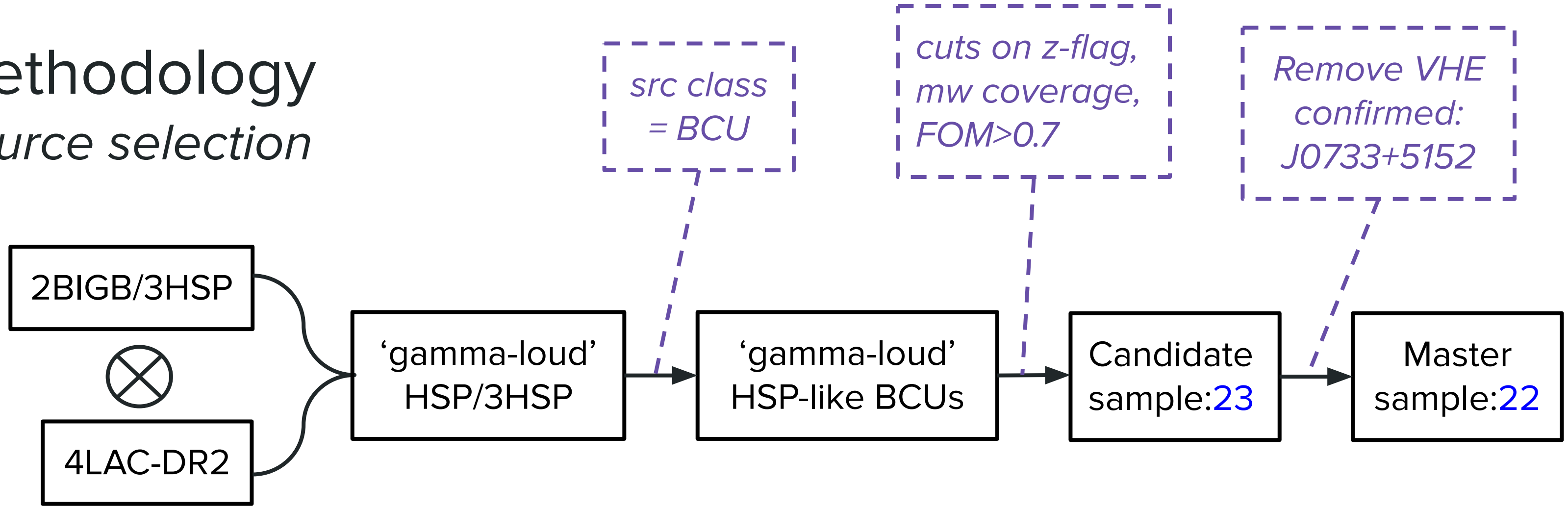

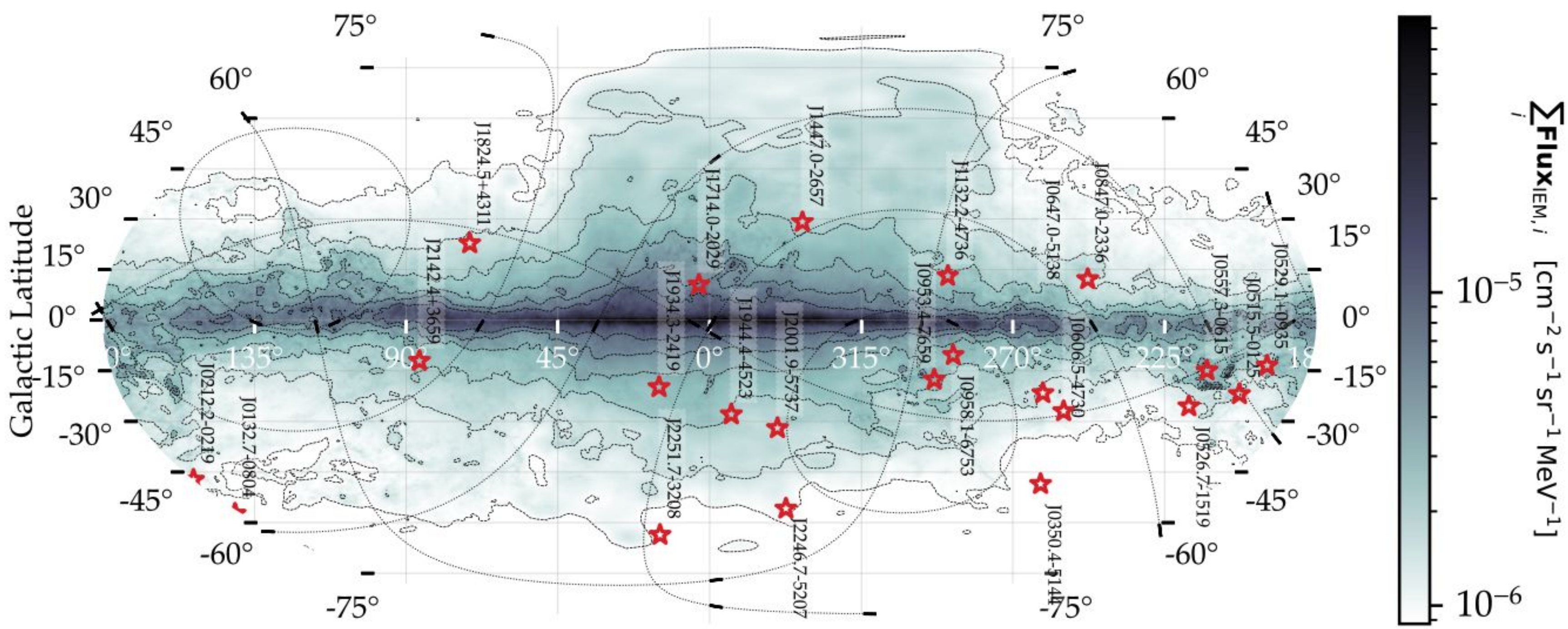

Methodology

Redshift determination

1 4LAC-DR2 redshifts
base redshifts

2 Chang et al. 2019 (3HSP)
photo-z, elliptical host galaxy

3 Goldoni et al. 2021
refined

Table 1. Master sample as obtained from 2BIGB.

4FGL Name	RAJ2000	DEJ2000	z	TS	FOM
J0132.7−0804	23.183	-8.074	0.148	88	0.8
J0212.2−0219	33.066	-2.319	0.250	61	0.8
J0350.4−5144	57.613	-51.743	0.32h	98	0.8
J0515.5−0125	78.891	-1.419	0.25h	55	0.8
J0526.7−1519	81.692	-15.321	0.21h	218	1.6
J0529.1+0935	82.297	9.597	0.30h	86	1.3
J0557.3−0615	89.344	-6.265	0.29h	53	1.6
J0606.5−4730	91.642	-47.504	0.030	137	1.0
J0647.0−5138	101.773	-51.638	0.22h	81	2.5
J0733.4+5152†	113.362	51.880	0.065	162	2.5
J0847.0−2336	131.757	-23.614	0.059	921	0.8
J0953.4−7659	148.367	-76.993	0.25h	104	0.8
J0958.1−6753	149.534	-67.894	0.21h	29	1.0
J1132.2−4736	173.056	-47.613	0.21h	129	1.0
J1447.0−2657	221.765	-26.962	0.32h	46	2.0
J1714.0−2029	258.522	-20.486	0.09h	110	2.0
J1824.5+4311	276.126	43.196	0.487	99	0.8
J1934.3−2419	293.582	-24.326	0.23h	63	1.6
J1944.4−4523	296.101	-45.393	0.21h	164	1.0
J2001.9−5737	300.491	-57.631	0.26h	123	0.8
J2142.4+3659	325.602	36.986	0.24h	110	1.3
J2246.7−5207	341.682	-52.126	0.098	95	2.5
J2251.7−3208	342.944	-32.140	0.246	52	2.0

Recently detected by MAGIC

Methodology

Archival radio, optical and X-ray data

We used SSDC's SED Builder: https://tools.ssdc.asi.it/SED/

- ❖ Search radius: of 5 arcmin (centred at low-energy counterpart position)
- ❖ No time-constraints (variability check performed)
- ❖ In case of doubt, we picked the source with better spectral coverage and checked the sanity of the resulting SED by eye.

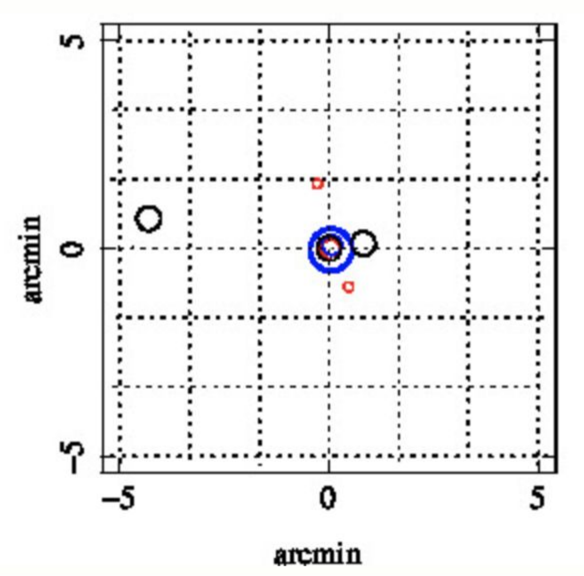

Methodology

Gamma-ray data analysis

Event selection and analysis:

- Pass 8 data from 100 MeV to 1.5 TeV, events within 20 deg radius (ROI).
- Same time cuts (GTIs) as 4FGL-DR2.
- Same event types / energy bins as in the 4FGL-DR2.
- Sky model: consider all sources in 4FGL-DR2 within 30 deg radius, fix parameters outside 8 deg except those with TS>25.
- <u>Use EBL Attenuated models</u> everywhere to improve GeV-TeV predictions.

Spectral models: LP and PWL with exponential cut-off (index Γ=1, as opposed to Γ=⅔ as in the 4FGL). Select best model using Akaike criterion.

$$\frac{\mathrm{d}N(E)}{\mathrm{d}E} = N_0 \left(\frac{E}{E_0}\right)^{-[\alpha+\beta\log(E/E_0)]} \mathrm{e}^{-[\tau_{\mathrm{EBL}}(z,E)+(E/E_{\mathrm{cut}})^{\Gamma}]}$$

M. Nievas Rosillo et al. (2022).

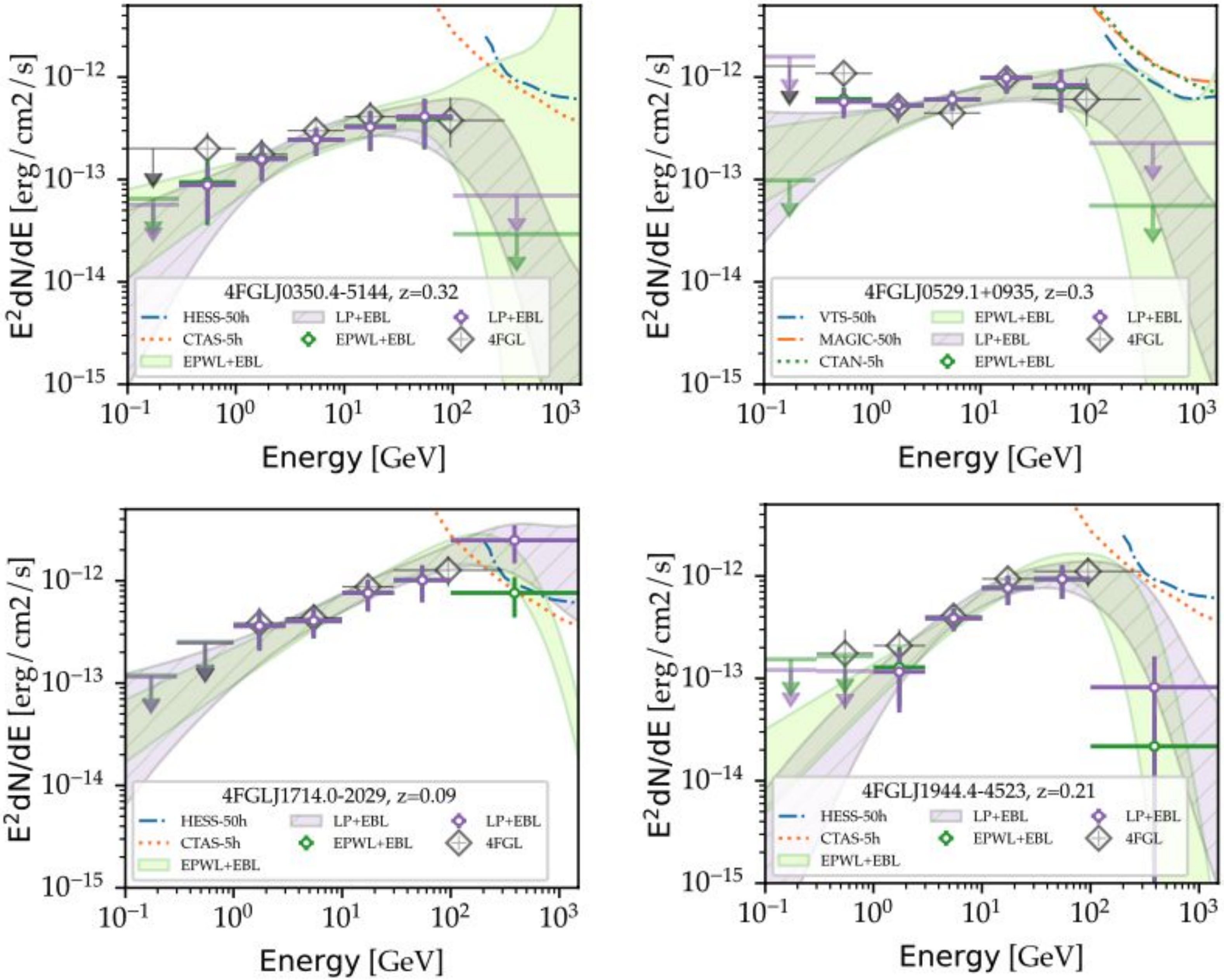

Broadband SED model

Base model: One-zone leptonic SSC model

+ host galaxy as a black-body emitter (approximate fit for giant ellipticals).
+ IR torus for sources with: a) very curved gamma-ray spectrum; b) hint of excess in the IR band.

Fixed parameters:

- $\gamma_{min} = 10^3$
- $\Gamma_{bulk} = 20$
- $R = 10^{16}$ cm
- $R_H = 10^{18}$ cm
- density of particles "N" normalized so that the integral of $n(\gamma)d\gamma$ from γ_{min} to γ_{max} is equal to 1.

The rest are minimized using *jetset*'s optimization tool with Minuit as minimizer. Since the number of free parameters is 9 (12 for sources with IR torus), i.e. high degeneracy. We found solutions that reproduce the SEDs, but might not be unique ...

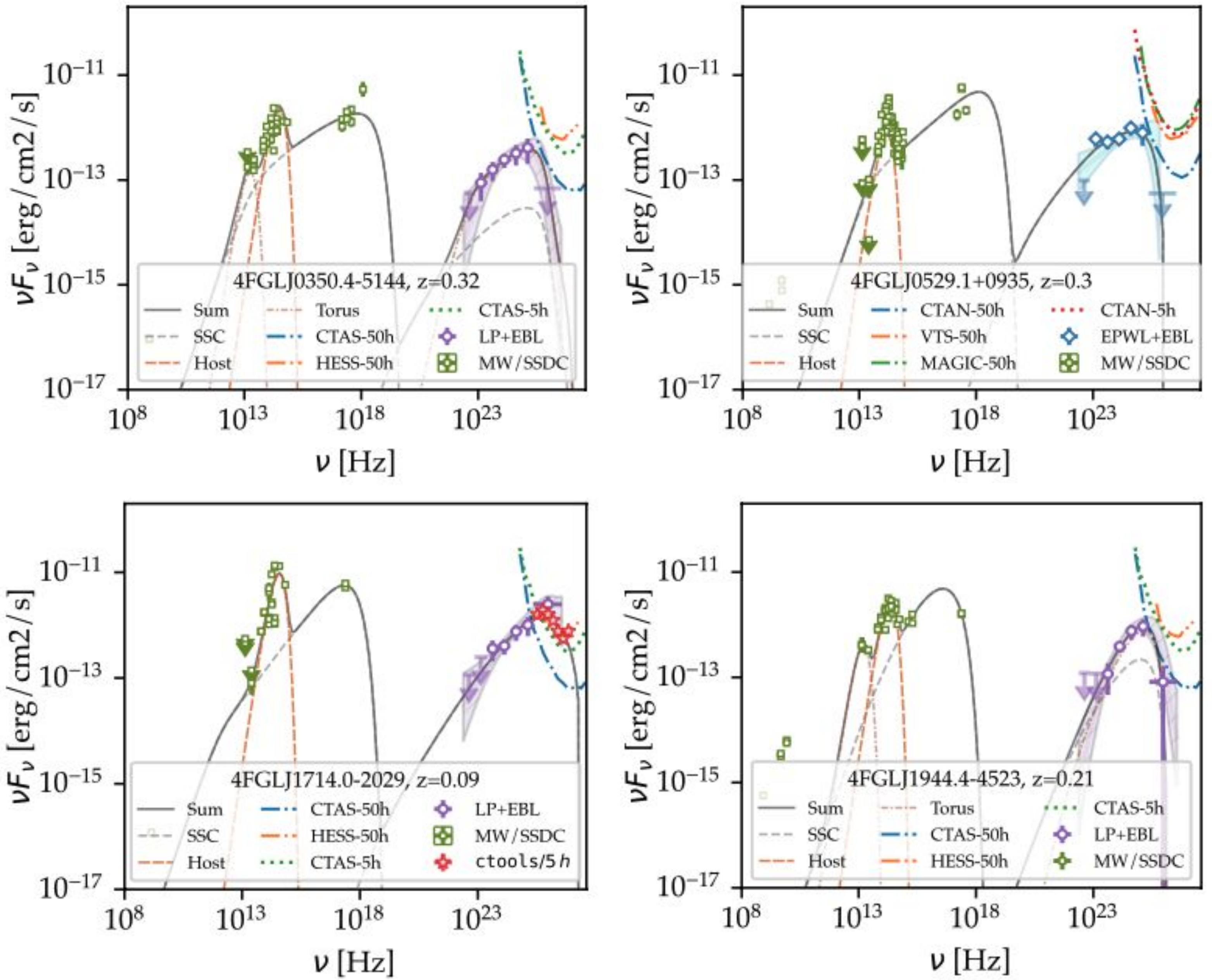
4FGLJ0350.4-5144, z=0.32
Sum
SSC
Host
Torus
CTAS-50h
HESS-50h
CTAS-5h
LP+EBL
MW/SSDC
4FGLJ0529.1+0935, z=0.3
Sum
SSC
Host
CTAN-50h
VTS-50h
MAGIC-50h
CTAN-5h
EPWL+EBL
MW/SSDC
4FGLJ1714.0-2029, z=0.09
Sum
SSC
Host
CTAS-50h
HESS-50h
CTAS-5h
LP+EBL
MW/SSDC
ctools/5h
4FGLJ1944.4-4523, z=0.21
Sum
SSC
Host
Torus
CTAS-50h
HESS-50h
CTAS-5h
LP+EBL
MW/SSDC
νFν [erg/cm2/s]
ν [Hz]

Results

Broadband emission:

All sources successfully reproduced using 1 zone SSC + EC (in some cases).

EHSP candidates (according to the broadband SED model) and properties:

Out of the 22 sources, *17 are classified as EHSPs* (ν_{sync} > 10^{17} Hz) and 5 as HSPs.

Gamma-ray variability:

Only J1714.0-2029 is marked as clearly variable (4FGL-DR2's Var. Index of 22.72, F_{var} = 0.69±0.31)

VHE emission: J0847.0-2336 and J1714.0-2029 detectable by IACTs (using CTA's Prod3b-v2 IRFs / Omega configuration 5h ≈ 50h with MAGIC/VERITAS/H.E.S.S.)

Properties of the sources

M. Nievas Rosillo et al. (2022).

- Low fluxes and hard spectra compared with other BL Lacs.
- Low variability compared to other blazars with similar fluxes.
- Only two VHE candidates out of 22 (surprising!).
- We find our sources in equipartition ($U_B \approx U_e$) **except** for the 2 VHE candidates, which have unusually low magnetization.

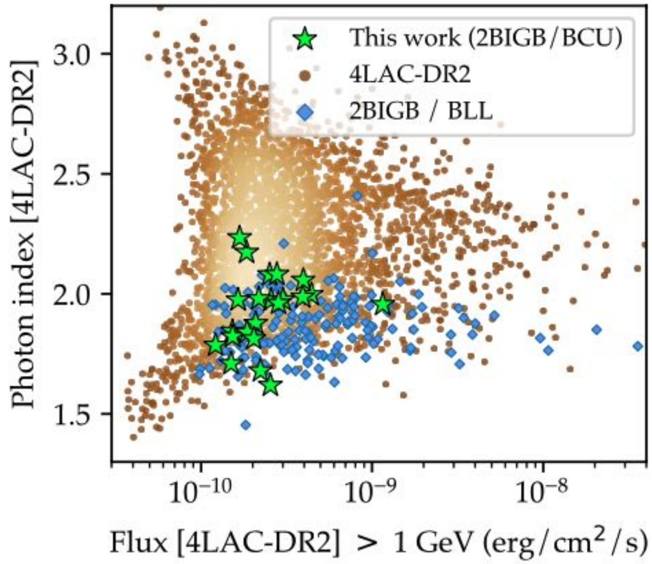

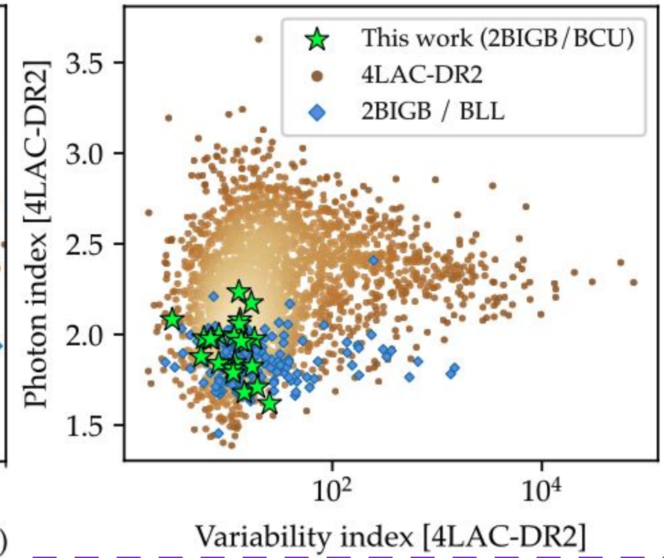

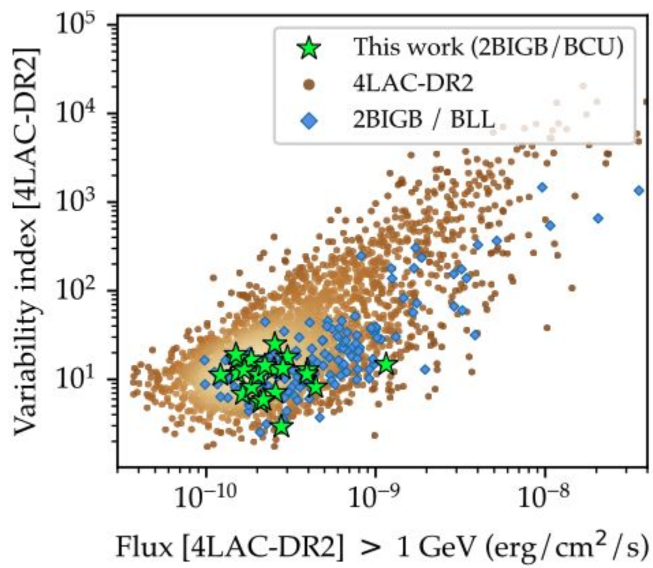

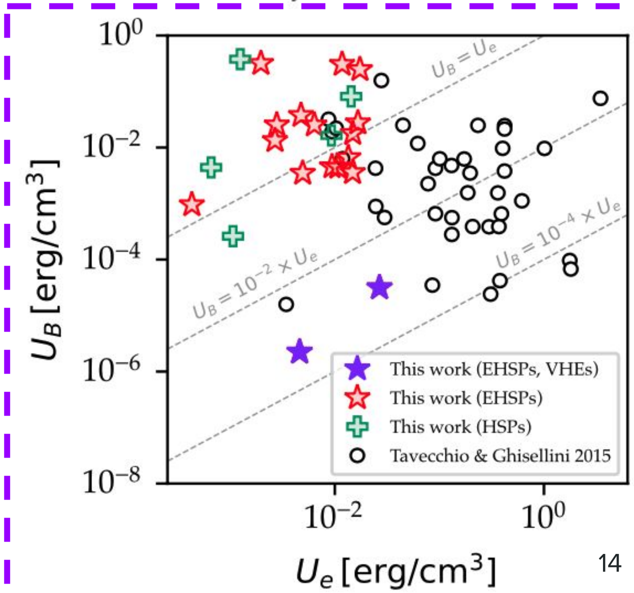

Conclusions

- Data-driven method to classify blazar candidates of unknown type.
- The data selection cuts are efficient selecting EHSPs: 17/22.
- One-zone SSC reproduces the broadband SED, except for the radio band.
- Host galaxy clearly visible: better redshift estimates likely doable.
- 4 sources with extreme synchrotron peak frequencies ($> 10^{18}$ Hz).
- VHE emission predictions based on broadband photometry (no Fermi extrapolation).
- Only 2 VHE candidates and they have very low magnetization (similar to what Tavecchio & Ghisellini (2015) found for other HSPs).

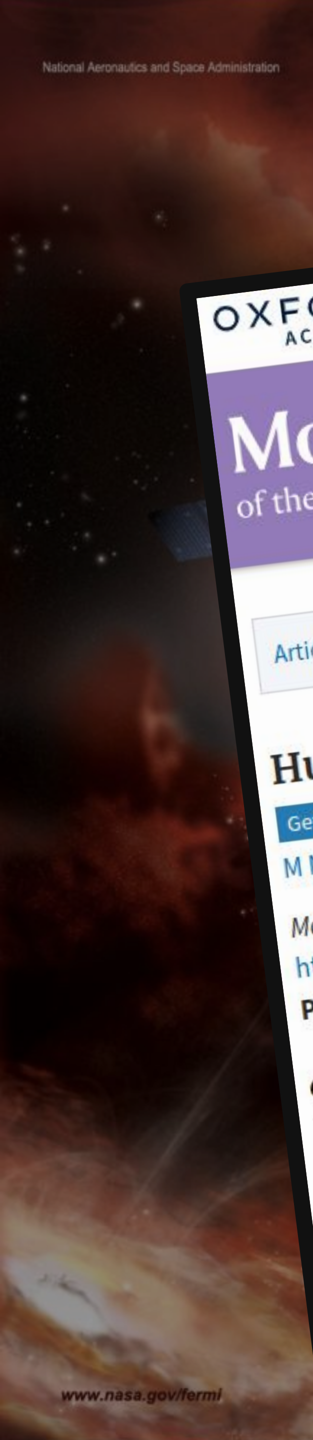

BL
ith


OXFORD ACADEMIC

Monthly Notices of the Royal Astronomical Society

Royal Astronomical Society

Article Navigation

Hunting extreme BL Lacertae blazars with Fermi-Large Area Telescope

Get access >

M Nievas Rosillo ✉, A Domínguez, G Chiaro, G La Mura, A Brill, V S Paliya

Monthly Notices of the Royal Astronomical Society, Volume 512, Issue 1, May 2022, Pages 137–159,
https://doi.org/10.1093/mnras/stac491
Published: 23 February 2022 **Article history** ▾

Cite Permissions Share ▾

ABSTRACT

The emission of very-high-energy (VHE) photons ($E > 100$ GeV) in blazars is closely connected to the production of ultra-relativistic particles and the role of these γ-ray sources as cosmic particle accelerators. This work focuses on a selection of 22 γ-ray objects from the 2BIGB catalogue of high-synchrotron-peaked

r. Ari Brill

https://confluence.slac.stanford.edu/display/SCIGRPS/Hunting+TeV+source+candidates+among+the+Fourth+Fermi-LAT+catalog

Backup

Why bother about EHSPs?

- The ***'least luminous'*** blazars***:*** more components are visible = richer physics.
- Inefficient Compton cooling (low accretion, naked AGN?) and ***particles acceleration operating at very high energies*** (Synchrotron peak in X-rays).
- ***Good targets for IACTs?*** (Inverse Compton peak expected in TeVs).
  - Good targets for ***EBL*** studies: 1) closeby, 2) with TeV emission? 3) Likely no cutoffs/Klein-Nishima softening/internal absorption, 4) low variability.
  - Good sources to study ***IGMFs***.
- ***Represent the end of the blazar sequence***. Dim in radio. AGN at the limit of shutting down?

However:

- Dim in HE γ-rays and hard spectrum: LAT is not optimal to detect them.
- Low variability means no bright flares: very long integrations needed.

Classical EHSPs: HESS J1943+213

THE ASTROPHYSICAL JOURNAL, 862:41 (15pp), 2018 July 20 Archer et al.

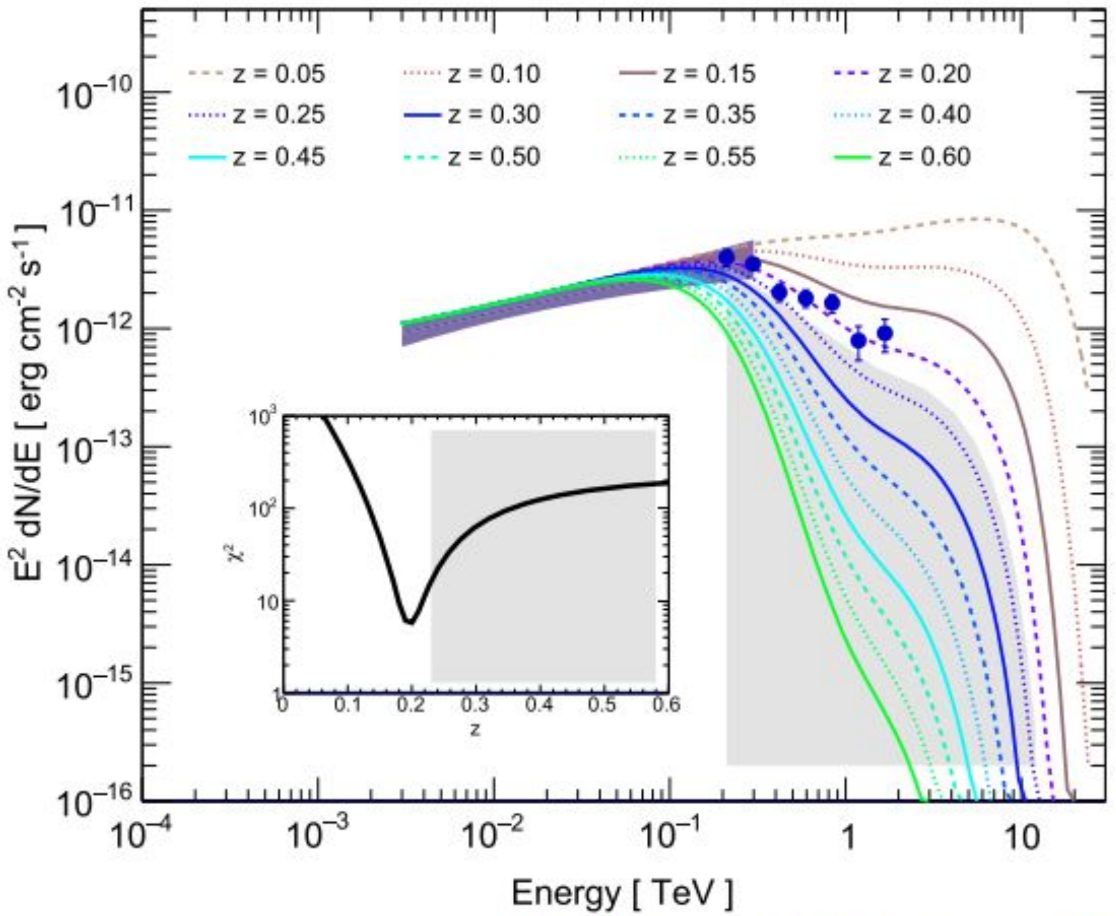

Figure 8. VERITAS observed spectrum (blue circles) fit to upper bound of the *Fermi*-LAT spectrum absorbed by EBL for redshift values ranging from 0 to 0.6. The inset shows the χ^2 distribution with redshift of the VERITAS spectrum fit to the EBL-absorbed extrapolations of the *Fermi*-LAT upper bound. The gray shaded areas show the 95% rejection regions.

Classical EHSPs: 1ES 0229+200

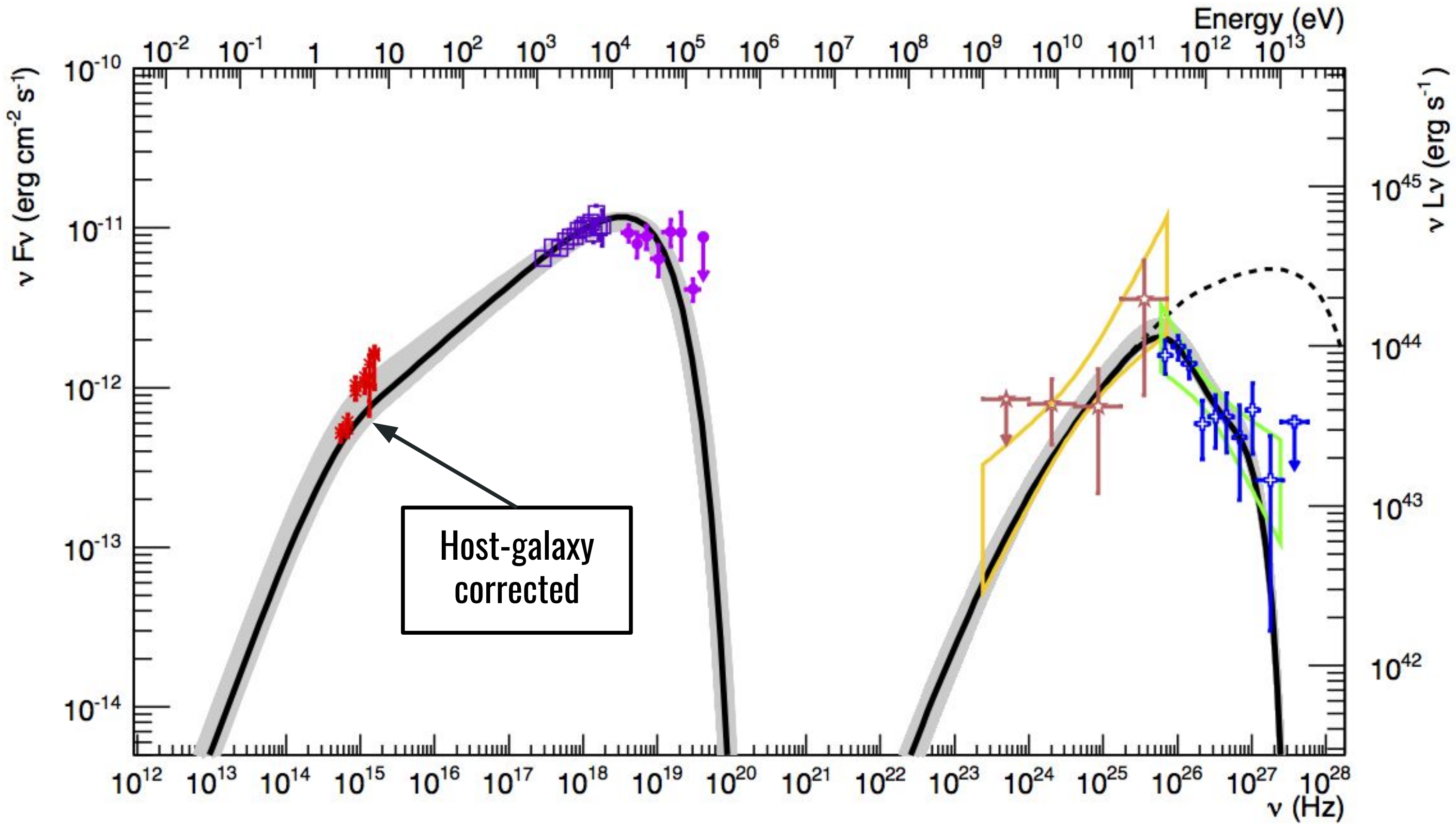

SED of 1ES 0229+200, one-zone SSC model.
VERITAS, ApJ 782: 13, 2014

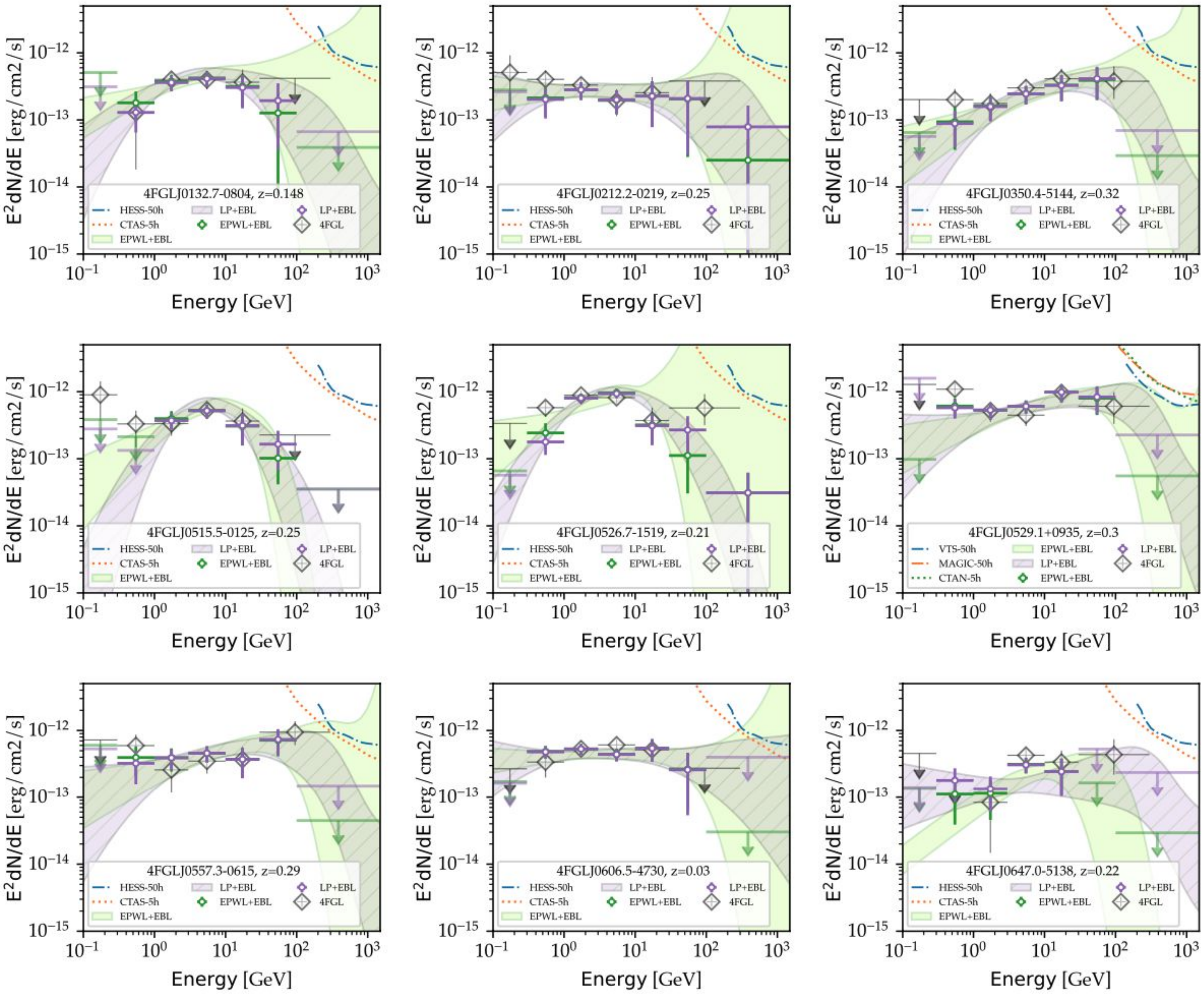

4FGLJ0132.7-0804, z=0.148
4FGLJ0212.2-0219, z=0.25
4FGLJ0350.4-5144, z=0.32
4FGLJ0515.5-0125, z=0.25
4FGLJ0526.7-1519, z=0.21
4FGLJ0529.1+0935, z=0.3
4FGLJ0557.3-0615, z=0.29
4FGLJ0606.5-4730, z=0.03
4FGLJ0647.0-5138, z=0.22
HESS-50h
CTAS-5h
VTS-50h
MAGIC-50h
CTAN-5h
EPWL+EBL
LP+EBL
4FGL
E^2dN/dE [erg/cm2/s]
Energy [GeV]

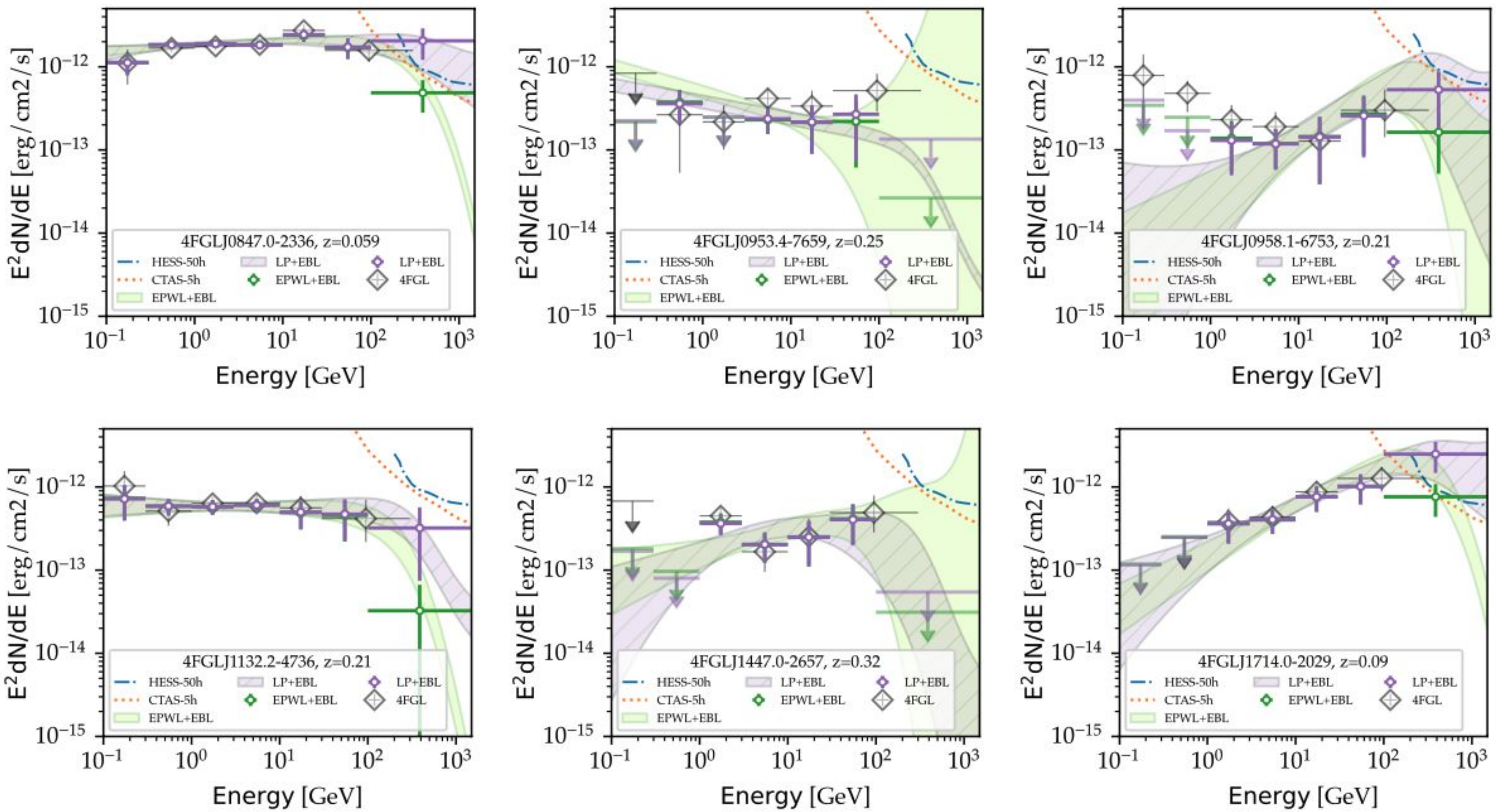
4FGLJ0847.0-2336, z=0.059
4FGLJ0953.4-7659, z=0.25
4FGLJ0958.1-6753, z=0.21
4FGLJ1132.2-4736, z=0.21
4FGLJ1447.0-2657, z=0.32
4FGLJ1714.0-2029, z=0.09
HESS-50h
CTAS-5h
EPWL+EBL
LP+EBL
4FGL
E²dN/dE [erg/cm2/s]
Energy [GeV]

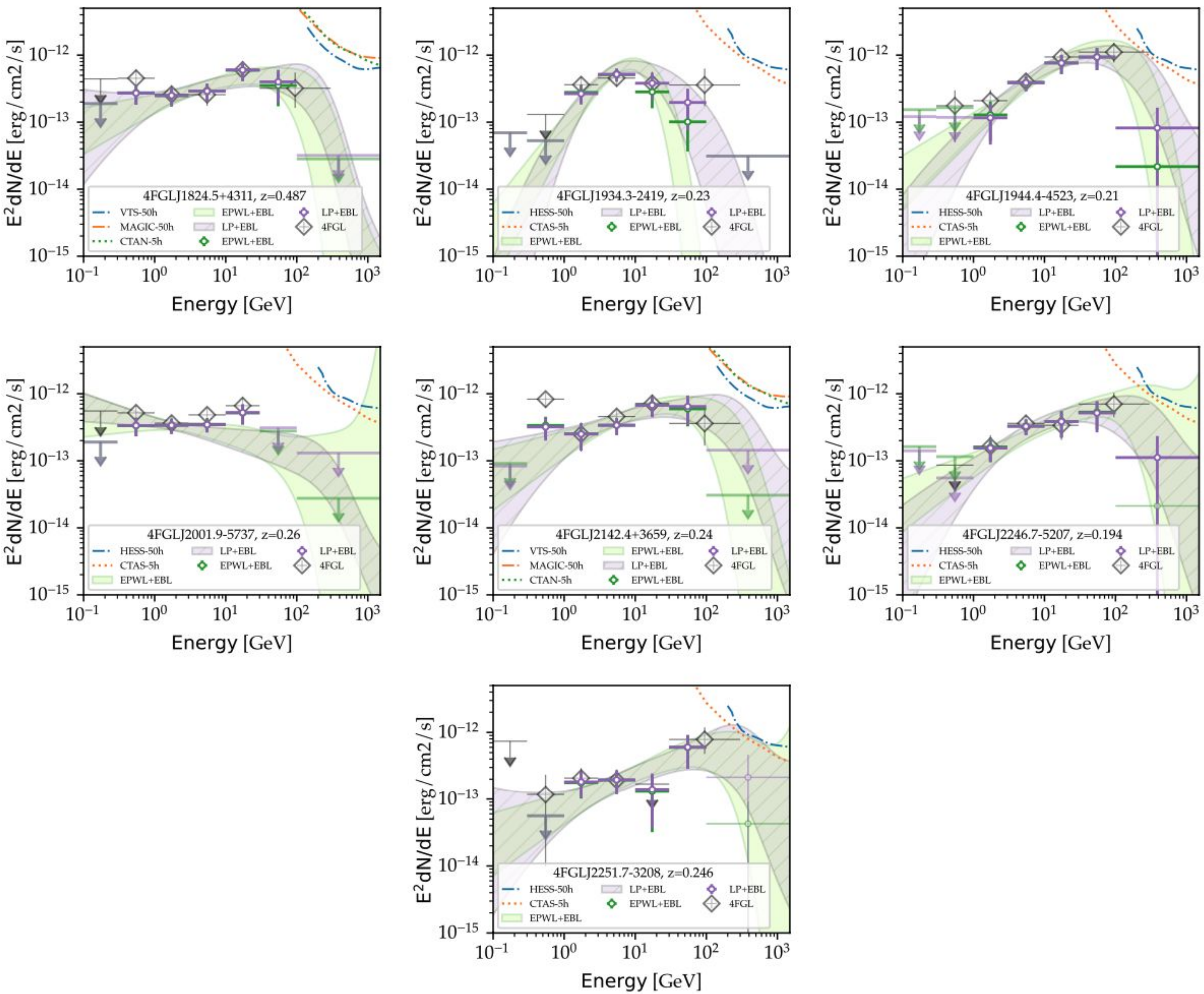
4FGLJ1824.5+4311, z=0.487
VTS-50h
MAGIC-50h
CTAN-5h
EPWL+EBL
LP+EBL
EPWL+EBL
LP+EBL
4FGL
4FGLJ1934.3-2419, z=0.23
HESS-50h
CTAS-5h
EPWL+EBL
LP+EBL
EPWL+EBL
LP+EBL
4FGL
4FGLJ1944.4-4523, z=0.21
HESS-50h
CTAS-5h
EPWL+EBL
LP+EBL
EPWL+EBL
LP+EBL
4FGL
4FGLJ2001.9-5737, z=0.26
HESS-50h
CTAS-5h
EPWL+EBL
LP+EBL
EPWL+EBL
LP+EBL
4FGL
4FGLJ2142.4+3659, z=0.24
VTS-50h
MAGIC-50h
CTAN-5h
EPWL+EBL
LP+EBL
EPWL+EBL
LP+EBL
4FGL
4FGLJ2246.7-5207, z=0.194
HESS-50h
CTAS-5h
EPWL+EBL
LP+EBL
EPWL+EBL
LP+EBL
4FGL
4FGLJ2251.7-3208, z=0.246
HESS-50h
CTAS-5h
EPWL+EBL
LP+EBL
EPWL+EBL
LP+EBL
4FGL
E²dN/dE [erg/cm2/s]
Energy [GeV]

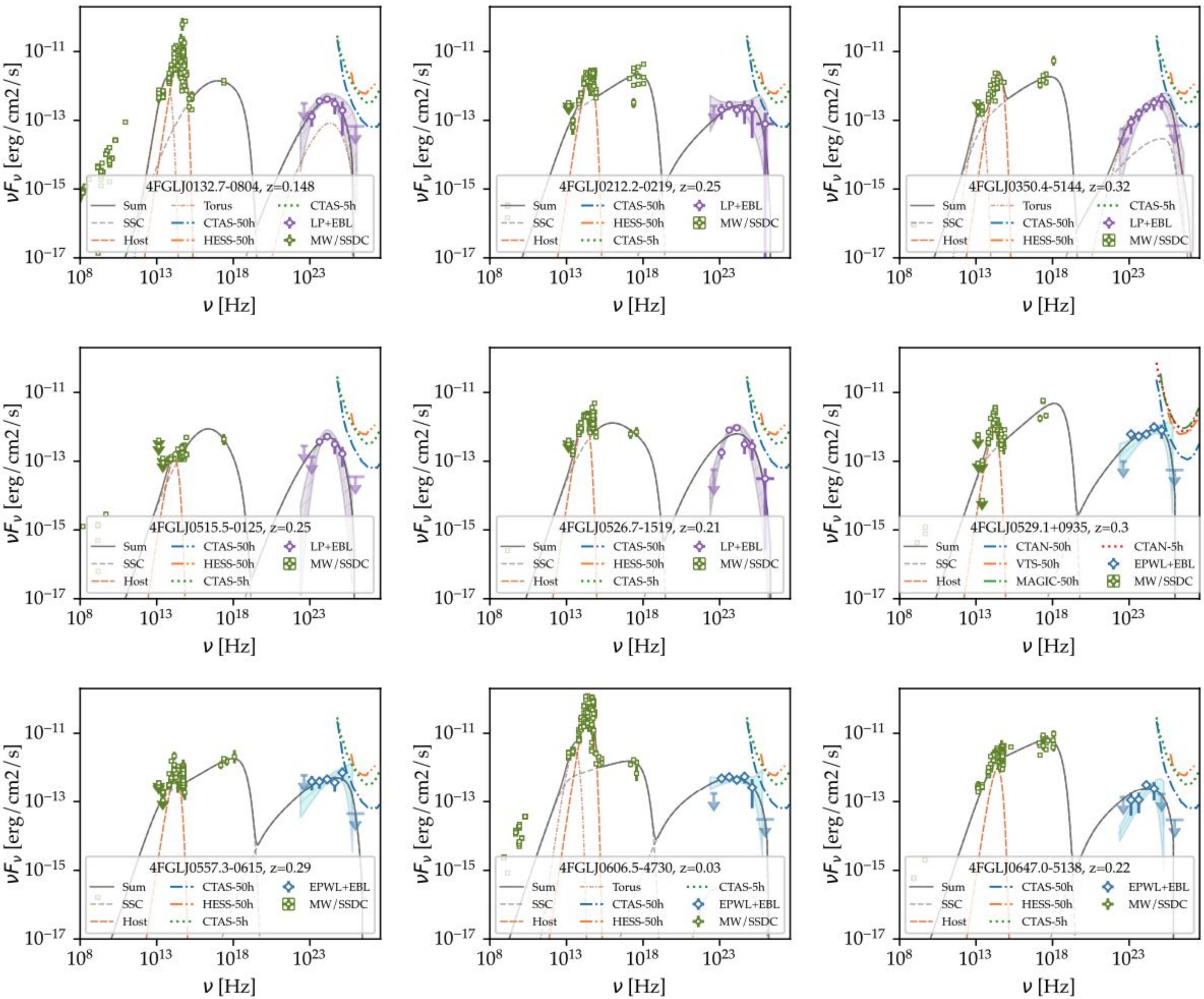
4FGLJ0132.7-0804, z=0.148
Sum
SSC
Host
Torus
CTAS-50h
HESS-50h
CTAS-5h
LP+EBL
MW/SSDC
4FGLJ0212.2-0219, z=0.25
Sum
SSC
Host
CTAS-50h
HESS-50h
CTAS-5h
LP+EBL
MW/SSDC
4FGLJ0350.4-5144, z=0.32
Sum
SSC
Host
Torus
CTAS-50h
HESS-50h
CTAS-5h
LP+EBL
MW/SSDC
4FGLJ0515.5-0125, z=0.25
Sum
SSC
Host
CTAS-50h
HESS-50h
CTAS-5h
LP+EBL
MW/SSDC
4FGLJ0526.7-1519, z=0.21
Sum
SSC
Host
CTAS-50h
HESS-50h
CTAS-5h
LP+EBL
MW/SSDC
4FGLJ0529.1+0935, z=0.3
Sum
SSC
Host
CTAN-50h
VTS-50h
MAGIC-50h
CTAN-5h
EPWL+EBL
MW/SSDC
4FGLJ0557.3-0615, z=0.29
Sum
SSC
Host
CTAS-50h
HESS-50h
CTAS-5h
EPWL+EBL
MW/SSDC
4FGLJ0606.5-4730, z=0.03
Sum
SSC
Host
Torus
CTAS-50h
HESS-50h
CTAS-5h
EPWL+EBL
MW/SSDC
4FGLJ0647.0-5138, z=0.22
Sum
SSC
Host
CTAS-50h
HESS-50h
CTAS-5h
EPWL+EBL
MW/SSDC
νF_ν [erg/cm2/s]
ν [Hz]

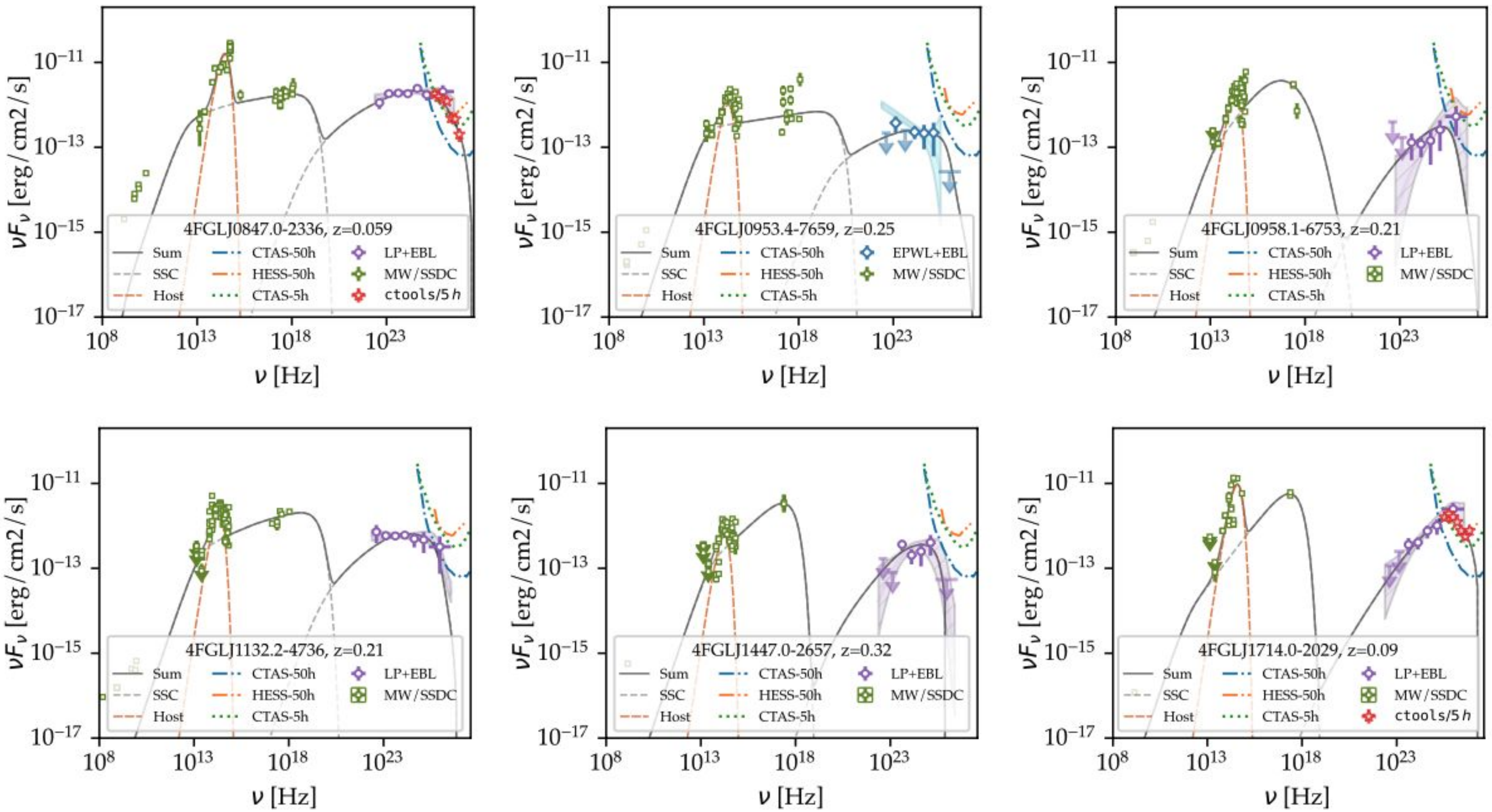
4FGLJ0847.0-2336, z=0.059
Sum
SSC
Host
CTAS-50h
HESS-50h
CTAS-5h
LP+EBL
MW/SSDC
ctools/5h
4FGLJ0953.4-7659, z=0.25
EPWL+EBL
4FGLJ0958.1-6753, z=0.21
4FGLJ1132.2-4736, z=0.21
4FGLJ1447.0-2657, z=0.32
4FGLJ1714.0-2029, z=0.09
νF_ν [erg/cm2/s]
ν [Hz]

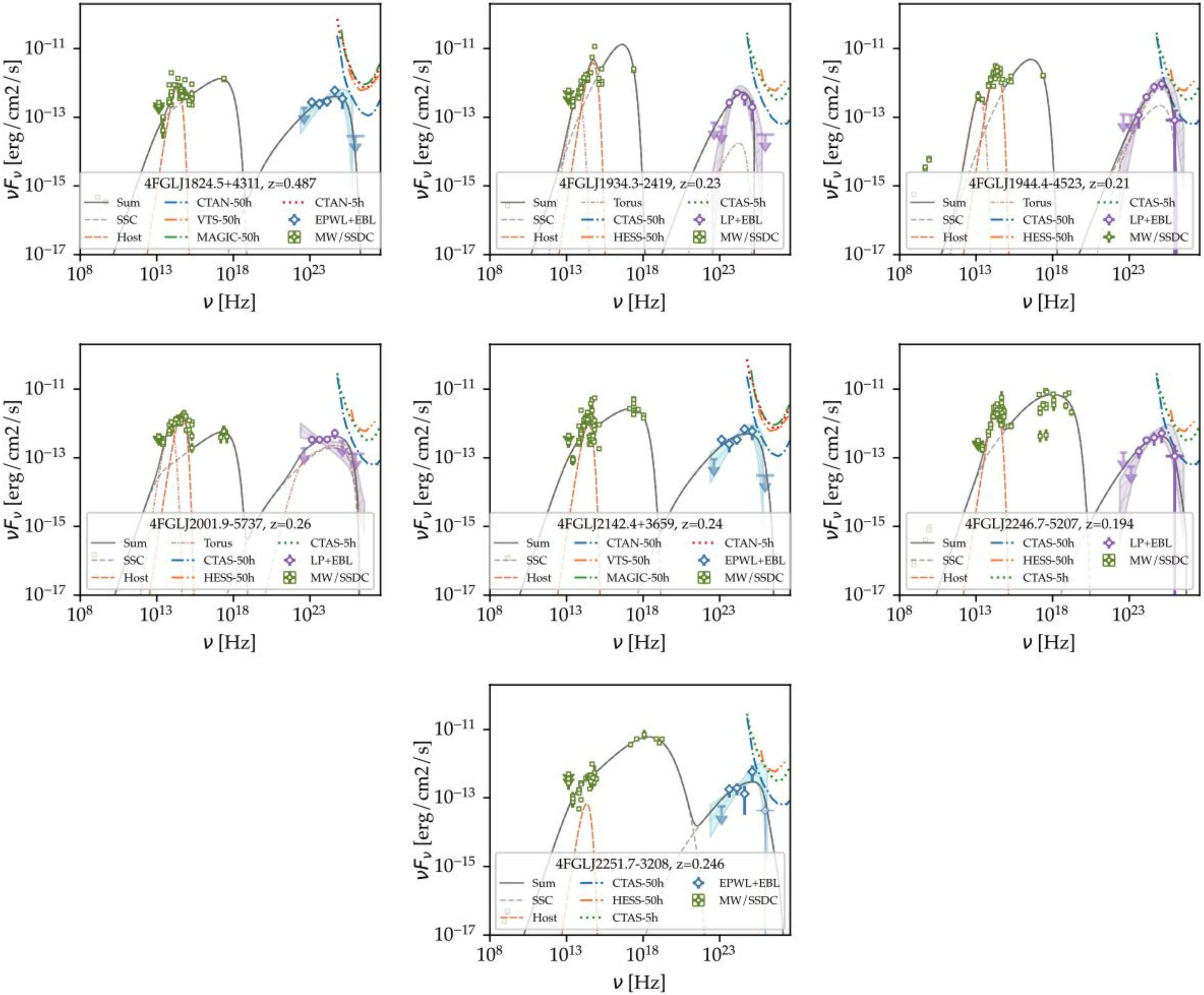
4FGLJ1824.5+4311, z=0.487
Sum
SSC
Host
CTAN-50h
VTS-50h
MAGIC-50h
CTAN-5h
EPWL+EBL
MW/SSDC
4FGLJ1934.3-2419, z=0.23
Torus
CTAS-50h
HESS-50h
CTAS-5h
LP+EBL
4FGLJ1944.4-4523, z=0.21
4FGLJ2001.9-5737, z=0.26
4FGLJ2142.4+3659, z=0.24
4FGLJ2246.7-5207, z=0.194
4FGLJ2251.7-3208, z=0.246
νF_ν [erg/cm2/s]
ν [Hz]

The ‘choice’ of γ_{min}

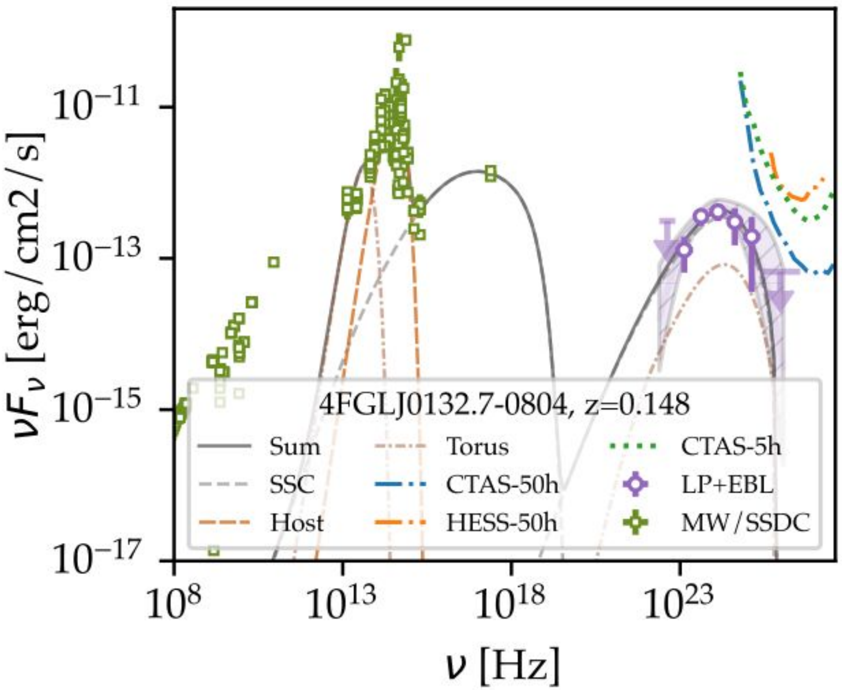

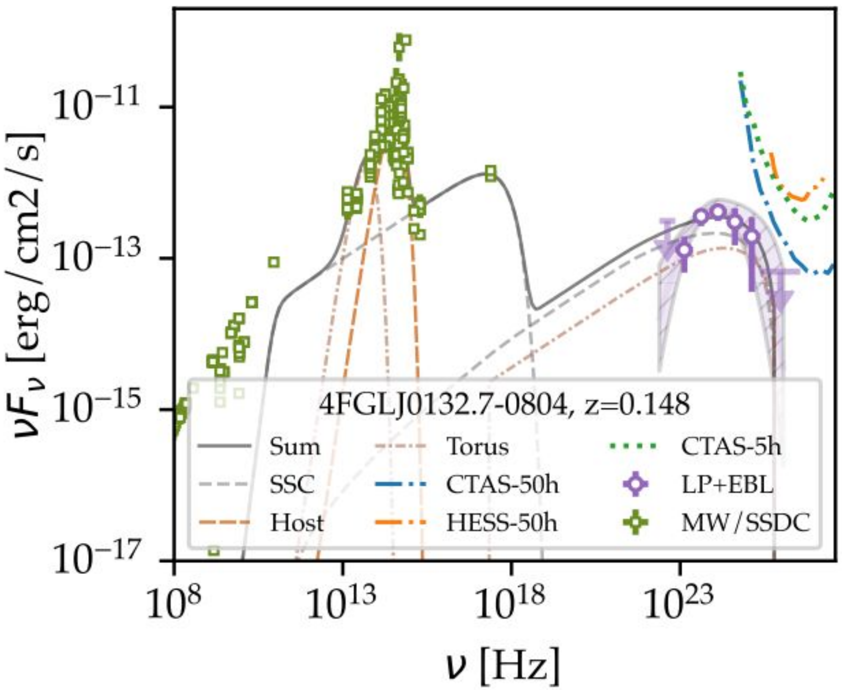

$\gamma_{min} = 10^3$

$\gamma_{min} = 1$

The ‘choice’ of γ_{min}

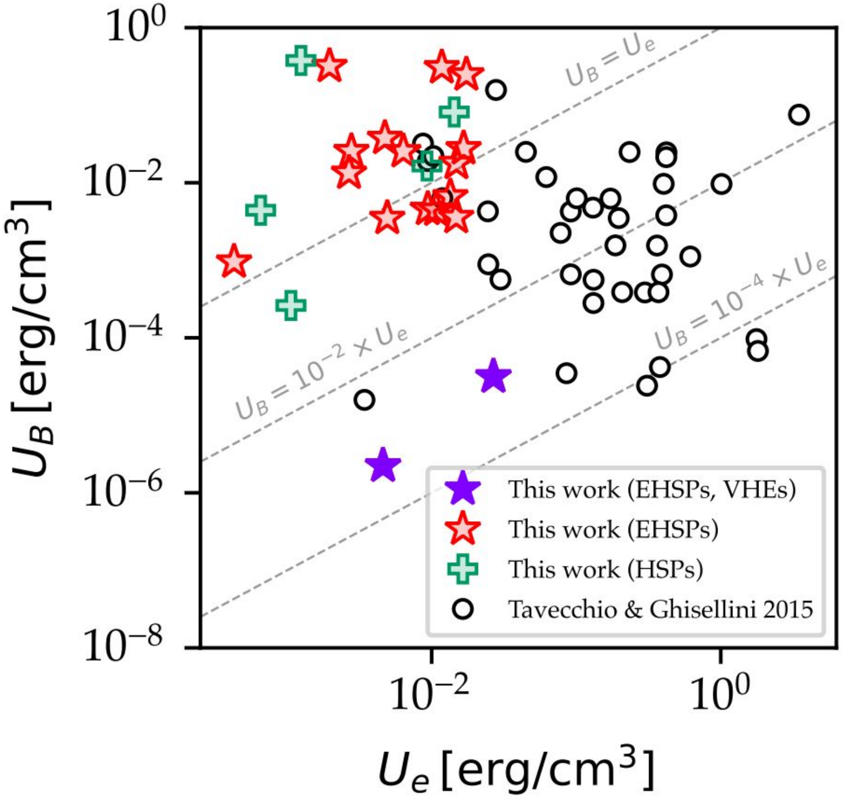

$\gamma_{\mathrm{min}} = 10^3$

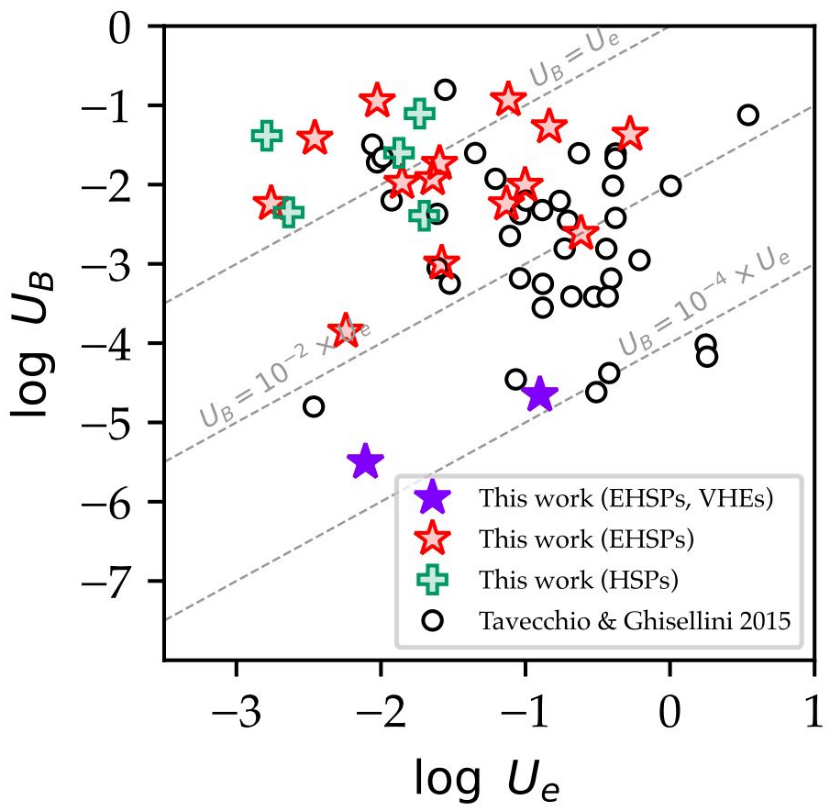

$\gamma_{\mathrm{min}} = 1$

About J0733.4+5152: sanity check

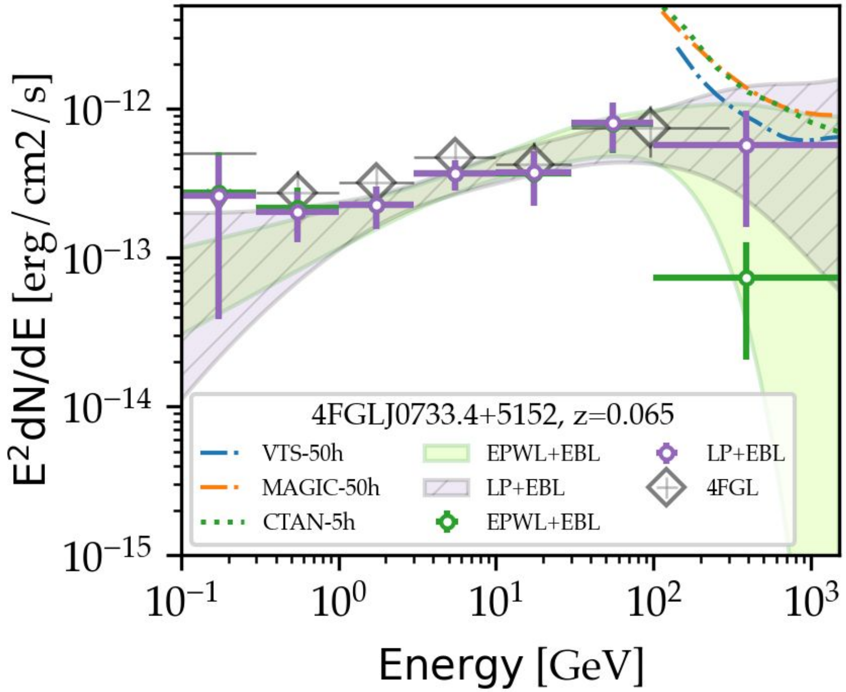

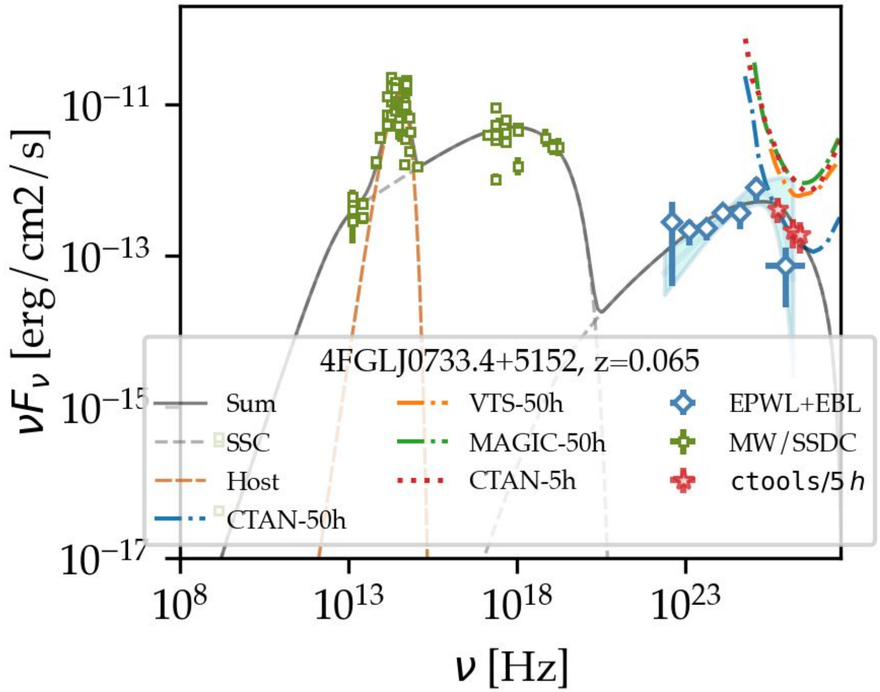

Hint of detection with our method ... note that MAGIC's detection paper claims a *harder-when-brighter* for X-ray data: during elevated state X-rays and gamma-rays may be enhanced.

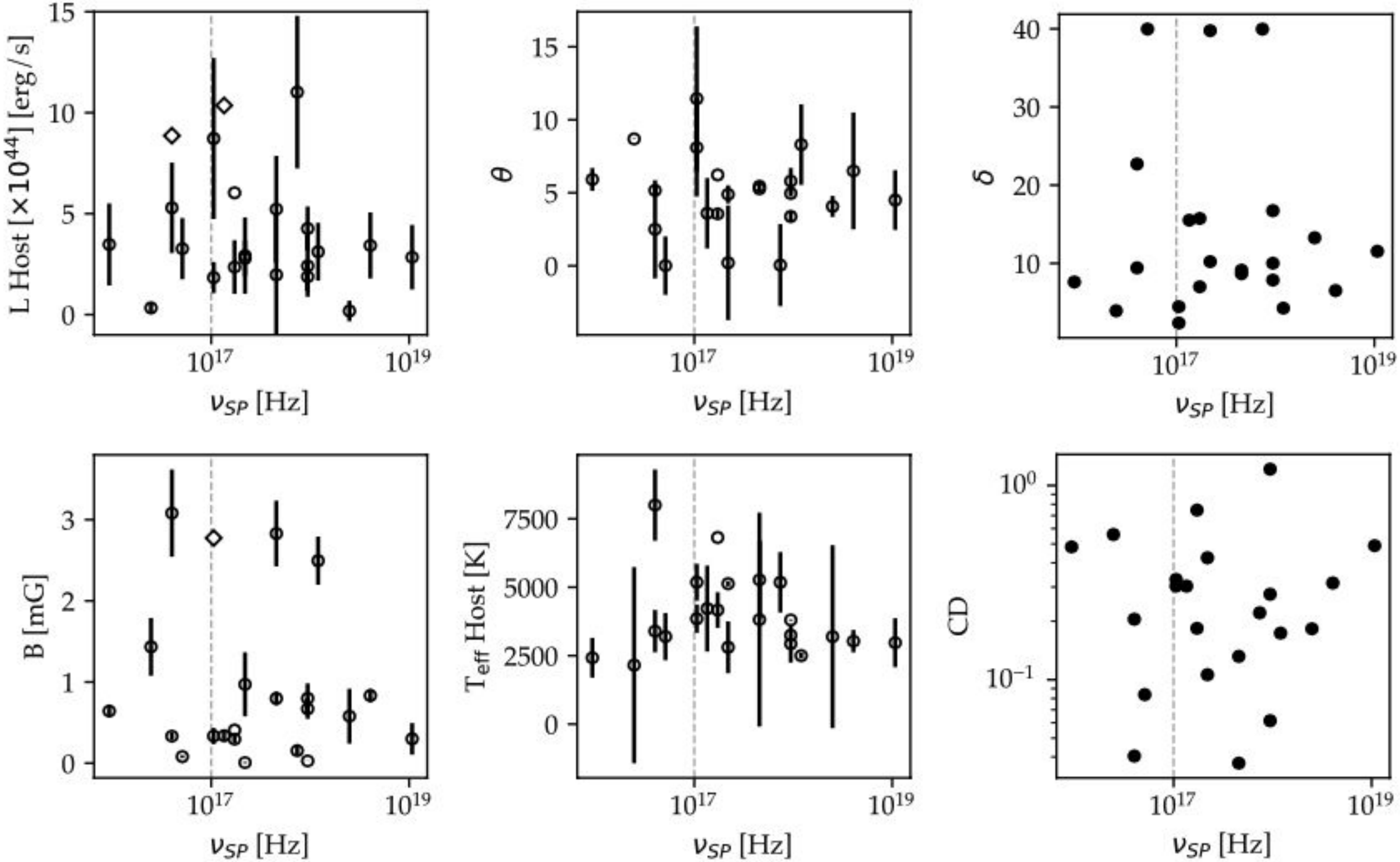

Figure 3. Best fit parameters

M. Nievas Rosillo et al. (2022)

Results

Modeling parameters

Table 3. Main jet model best-fit parameters, including electron density N, magnetic field strength B, electron indices before and after the break p_1 and p_2, maximum Lorentz factors γ_{max} and position of the spectral break γ_{br}, jet angle with respect to the line of sight θ, Doppler boosting δ, estimated position of the synchrotron peak ν_{SP}, favored LAT model to reproduce the high energy data: Log Parabola (LP) or Power Law with exponential cut-off (EPWL), Compton dominance (CD) and the classification as either HSP or EHSP. Fixed values: radius of the emitting region $R = 1.0 \times 10^{16}$ cm, position with respect to the central object $R_H = 2.0 \times 10^{18}$ cm. Bulk Lorentz factor is fixed to $\Gamma = 20$. Assumed minimum Lorentz factor $\gamma_{min} = 10^3$. [†] denotes unconstrained best-fit parameters.

4FGL Name	N (cm^{-3})	B (G)	p_1	p_2	γ_{br} [$\times 10^4$]	γ_{max} [$\times 10^6$]	θ (deg)	δ	log ν_{SP} [Hz]	LAT model	CD	Class
J0132.7−0804	0.04[†]	2.8 ± 1.6	0.65 ± 0.08	4.0 ± 2.5	3.0 ± 1.6	0.35 ± 0.21	11 ± 5	2.4	17.0	LP	0.3	EHSP
J0212.2−0219	(6.2 ± 0.9) × 10^4	0.80 ± 0.08	2.413 ± 0.013	4.2 ± 1.6	0.4 × 10^3[†]	0.30 ± 0.05	5.4 ± 0.4	8.7	17.7	LP	0.13	EHSP
J0350.4−5144	(5 ± 4) × 10^1	0.15 ± 0.06	1.831 ± 0.015	2.55 ± 0.21	0.5[†]	0.40 ± 0.20	0.1[†]	40	17.9	LP	0.22	EHSP
J0515.5−0125	0.006 ± 0.004	1.4 ± 0.4	0.38 ± 0.07	6.0 ± 0.9	4.4 ± 1.4	0.2841 ± 0.0024	8.7[†]	3.9	16.4	LP	0.56	HSP
J0526.7−1519	0.001[†]	0.64 ± 0.07	0.06[†]	4.0 ± 0.4	0.87 ± 0.32	0.40 ± 0.22	5.9 ± 0.8	7.6	16.0	LP	0.48	HSP
J0529.1+0935	0.6 × 10^4 [†]	2.49 ± 0.30	1.9 ± 0.5	2.2 ± 0.7	0.01[†]	0.36 ± 0.10	8.3 ± 2.8	4.3	18.1	EPWL	0.17	EHSP
J0557.3−0615	(2.5 ± 0.7) × 10^5	0.67 ± 0.12	2.477 ± 0.026	2.5 ± 1.3	(2.1 ± 1.7) × 10^3	0.5[†]	5.8 ± 0.9	7.9	18.0	EPWL	0.28	EHSP
J0606.5−4730	1 × 10^4 [†]	0.33 ± 0.10	1.9 ± 0.5	2.8 ± 0.8	0.05[†]	0.38 ± 0.05	8.1 ± 3.4	4.5	17.0	EPWL	0.33	EHSP
J0647.0−5138	(3.1 ± 0.9) × 10^3	2.8 ± 0.4	1.948 ± 0.031	2.59 ± 0.07	0.0[†]	0.155[†]	5.27[†]	9.1	17.7	EPWL	0.037	EHSP
J0733.4+5152	(3.0 ± 0.6) × 10^4	0.31 ± 0.14	2.417 ± 0.021	4.4 ± 0.6	(7 ± 6) × 10^1	1.47 ± 0.29	4.9 ± 0.4	10	17.9	EPWL	0.082	EHSP
J0847.0−2336	1.3 × 10^4 [†]	0.0281 ± 0.0020	1.90 ± 0.18	2.86 ± 0.26	0.18[†]	2.4 ± 1.5	3.4 ± 0.4	17	18.0	LP	1.2	EHSP
J0953.4−7659	(5.8 ± 2.0) × 10^6	0.30 ± 0.19	2.86 ± 0.07	2.9 ± 2.8	0.9 × 10^3[†]	3.00 ± 0.24	4.5 ± 2.0	12	19.0	EPWL	0.49	EHSP
J0958.1−6753	1 × 10^1 [†]	0.081 ± 0.016	1.6 ± 0.5	10 ± 4	38 ± 32	2.68 ± 0.22	0.0[†]	40	16.7	LP	0.084	HSP
J1132.2−4736	(2.9 ± 2.7) × 10^5	0.83 ± 0.08	2.468 ± 0.016	2.80 ± 0.12	2[†]	1.35 ± 0.07	6 ± 4	6.5	18.6	LP	0.31	EHSP
J1447.0−2657	0.6 × 10^4 [†]	1.0 ± 0.4	2.17 ± 0.17	4.3 ± 1.9	(3.2 ± 2.2) × 10^3	0.145[†]	4.9 ± 0.6	10	17.3	LP	0.11	EHSP
J1714.0−2029	123 ± 27	0.007[†]	1.810 ± 0.020	4.0 ± 1.4	0.5 × 10^3[†]	0.7[†]	0.0[†]	40	17.3	LP	0.42	EHSP
J1824.5+4311	(2.5 ± 1.9) × 10^3	0.34 ± 0.07	1.92 ± 0.09	2.41 ± 0.21	0.3[†]	0.2[†]	3.6 ± 2.4	16	17.1	EPWL	0.3	EHSP
J1934.3−2419	0.05[†]	3.1 ± 0.5	0.96 ± 0.19	2[†]	7[†]	0.0295 ± 0.0027	5.2 ± 0.4	9.4	16.6	LP	0.04	HSP
J1944.4−4523	1.2 × 10^{-4} [†]	0.33 ± 0.05	0.337 ± 0.033	6 ± 4	5.6 ± 0.8	0.08[†]	2.5[†]	23	16.6	LP	0.2	HSP
J2001.9−5737	6.323 × 10^4 [†]	0.408[†]	2.33[†]	2.48[†]	20.85[†]	0.276[†]	6.23[†]	7.0	17.2	LP	0.75	EHSP
J2142.4+3659	(4.2 ± 1.1) × 10^3	0.30 ± 0.05	2.115 ± 0.021	3.1 ± 0.6	7 ± 4	0.27 ± 0.24	3.56 ± 0.29	16	17.2	EPWL	0.18	EHSP
J2246.7−5207	54 ± 6	0.80 ± 0.18	1.702 ± 0.011	3.73 ± 0.15	12.7 ± 1.6	0.85 ± 0.11	4.96 ± 0.21	10	18.0	LP	0.061	EHSP
J2251.7−3208	(2.3 ± 1.0) × 10^3	0.58 ± 0.34	2.14 ± 0.05	11.9 ± 2.3	(3.9 ± 2.2) × 10^2	7.5 ± 1.1	4.1 ± 0.7	13	18.4	EPWL	0.18	EHSP

M. Nievas Rosillo et al. (2022)

Results

Energy budget and thermal components

Table 4. Energy budget, showing the effective temperature $T_{eff,host}$ of the black body that we added to simulate host galaxy emission, the effective temperature of the dusty torus T_{DT}, the integrated host luminosity L_{host} and the luminosity carried by the jet for the non-thermal low energy and total radiative components L_{sync} and L_{rad}, the electrons L_{kin}, the Poynting luminosity due to the magnetic field L_B, the total jet luminosity L_{tot} and the energy density ratio of the magnetic field to that of the electron distribution U_B/U_e. [†] denotes unconstrained best-fit parameters.

4FGL Name	R_{DT} [$\times 10^{18}$] (cm)	T_{DT} [$\times 10^2$] (K)	τ_{DT}	T_{host} [$\times 10^3$] (K)	L_{host} [$\times 10^{44}$] (erg/s)	L_{sync} [$\times 10^{42}$] (erg/s)	L_{rad} [$\times 10^{42}$] (erg/s)	L_B [$\times 10^{42}$] (erg/s)	L_{kin} [$\times 10^{44}$] (erg/s)	L_{tot} [$\times 10^{44}$] (erg/s)	U_B/U_e
J0132.7−0804	2.0[†]	6.1 ± 2.3	0.15[†]	5.2 ± 0.7	9 ± 4	1.7×10^3	1.1×10^3	2.0×10^3	0.44	33	26
J0212.2−0219	-	-	-	5.3 ± 1.4	5.2 ± 2.6	46	95	52	0.24	1.7	4.0
J0350.4−5144	13.1 ± 1.9	2.9 ± 1.3	0.063 ± 0.017	5.2 ± 1.1	11 ± 4	0.16	3.6	0.19	0.016	0.054	2.2
J0515.5−0125	-	-	-	2[†]	0.33 ± 0.29	3.8×10^2	3.0×10^2	5.6×10^2	0.54	9.3	5.7
J0526.7−1519	-	-	-	2.4 ± 0.7	3.5 ± 2.0	35	62	49	0.35	1.5	1.8
J0529.1+0935	-	-	-	2.50 ± 0.10	3.1 ± 1.4	2.2×10^3	9.3×10^2	2.6×10^3	0.65	37	14
J0557.3−0615	-	-	-	2.9 ± 0.7	2.4 ± 1.5	86	67	1.1×10^2	0.56	2.4	1.2
J0606.5−4730	$(1.0 \pm 0.8) \times 10^2$	4.3 ± 3.1	0.06[†]	3.8 ± 0.5	1.8 ± 0.8	7.4	17	9.7	0.4	0.67	0.42
J0647.0−5138	-	-	-	4[†]	2.0[†]	94	1.1×10^3	97	0.074	13	1.6×10^2
J0733.4+5152	-	-	-	4.43 ± 0.19	1.9 ± 0.9	3.9	14	4.3	0.11	0.3	1.3
J0847.0−2336	-	-	-	3.802 ± 0.024	1.9 ± 0.7	0.22	0.12	0.46	1.0	1.0	1.1×10^{-3}
J0953.4−7659	-	-	-	3.0 ± 0.9	2.8 ± 1.6	9.5	13	12	0.56	0.82	0.24
J0958.1−6753	-	-	-	3.2 ± 0.9	3.3 ± 1.5	0.12	0.98	0.12	0.04	0.051	0.25
J1132.2−4736	-	-	-	3.0 ± 0.4	3.4 ± 1.6	1.3×10^2	1.0×10^2	1.7×10^2	0.63	3.4	1.7
J1447.0−2657	-	-	-	2.8 ± 0.9	2.9 ± 1.9	54	1.4×10^2	61	0.18	2.2	7.9
J1714.0−2029	-	-	-	5.13 ± 0.09	2.8 ± 0.9	0.021	8.3×10^{-3}	0.031	0.17	0.17	4.8×10^{-4}
J1824.5+4311	-	-	-	4.2 ± 1.6	10 ± 6	12	17	16	0.35	0.69	0.49
J1934.3−2419	1.4[†]	8.4 ± 2.3	0.11 ± 0.09	8.0 ± 1.3	9 ± 8	94	1.4×10^3	98	0.047	15	3.0×10^2
J1944.4−4523	11[†]	2[†]	0.14 ± 0.12	3.4 ± 0.8	5.3 ± 2.2	1.0	17	1.2	0.025	0.2	6.7
J2001.9−5737	2[†]	12.3[†]	0.35[†]	6.8[†]	6.0[†]	29	25	54	0.51	1.3	0.49
J2142.4+3659	-	-	-	4.2 ± 0.7	2.4 ± 1.3	5.1	13	6.1	0.19	0.38	0.71
J2246.7−5207	-	-	-	3.24 ± 0.04	4.3 ± 1.1	53	96	55	0.1	1.6	9.1
J2251.7−3208	-	-	-	3.2[†]	0.2[†]	27	50	28	0.1	0.89	5.0

M. Nievas Rosillo et al. (2022)

Introduction.

Anatomy of an AGN

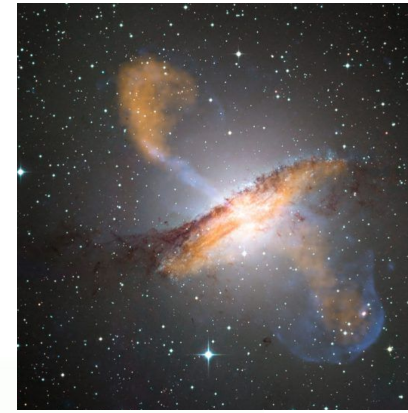

Radio Loud: blazar
Radio Quiet: quasar

RL: SSRQ
RQ: Sy 1

RL: radio galaxy

RQ: Sy 2

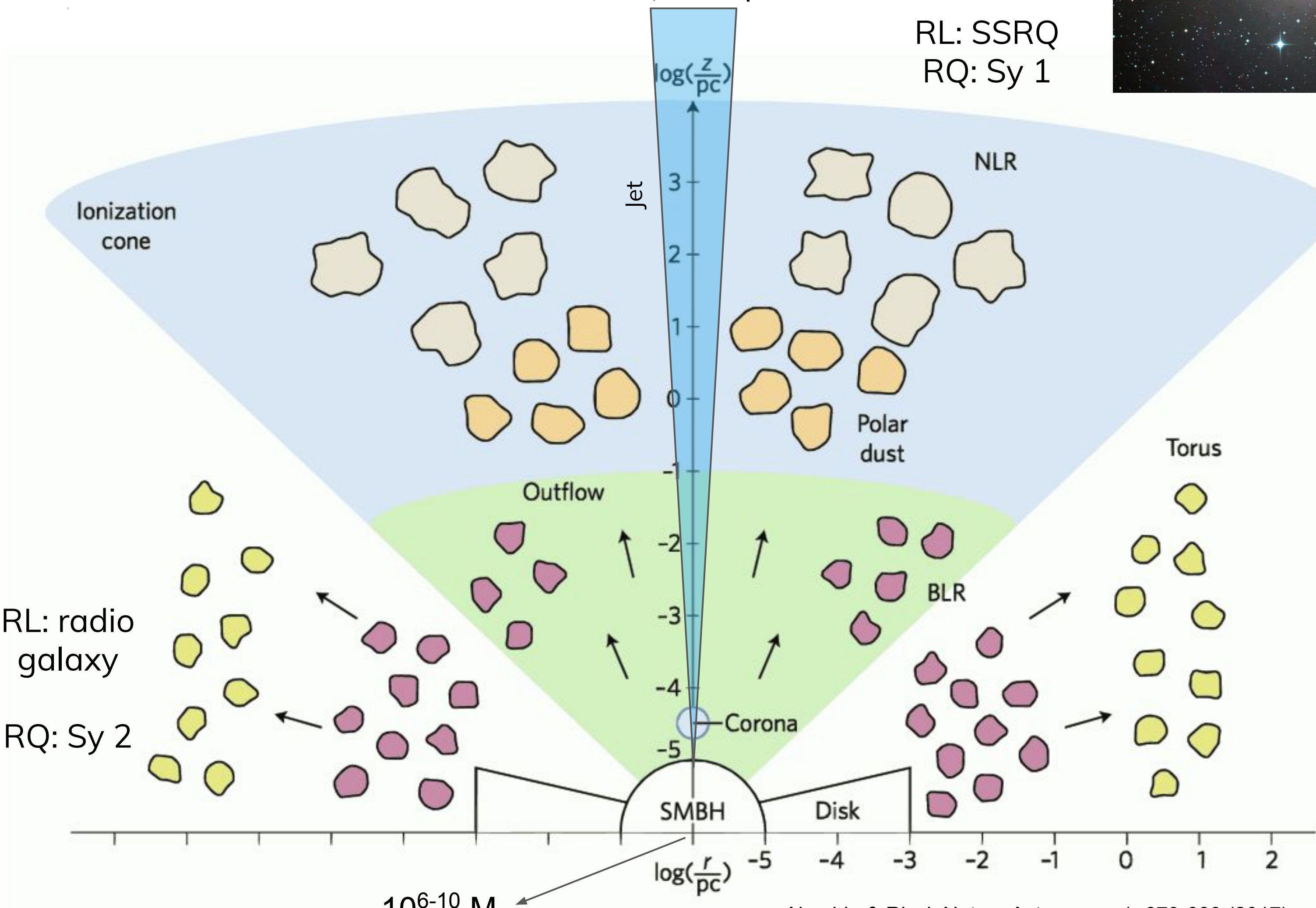

$10^{6\text{-}10}$ $M_{\odot}$

Almeida & Ricci, Nature Astronomy, 1, 679-689 (2017)

34

Shutting down the AGN emission...

Behind the non-thermal Synchrotron, AGNs hide other components: galaxy light, blue bump, torus, maybe starburst activity, etc.

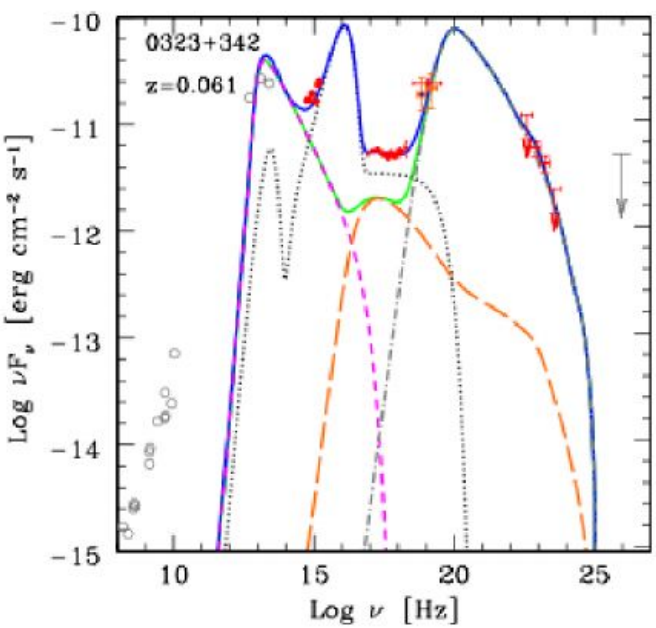

Spectral energy distribution of the NLSy1 galaxy 1H0323+342
Tibolla et al. ICRC 2013

AGN torus (purple), starburst (green), galaxy (yellow) and blue bump (blue) components. Red points show the total SEDs integrated across the filter bandpasses and the black points with error bars show the observed luminosities.
Williams et al. MNRAS 475(3) 2017

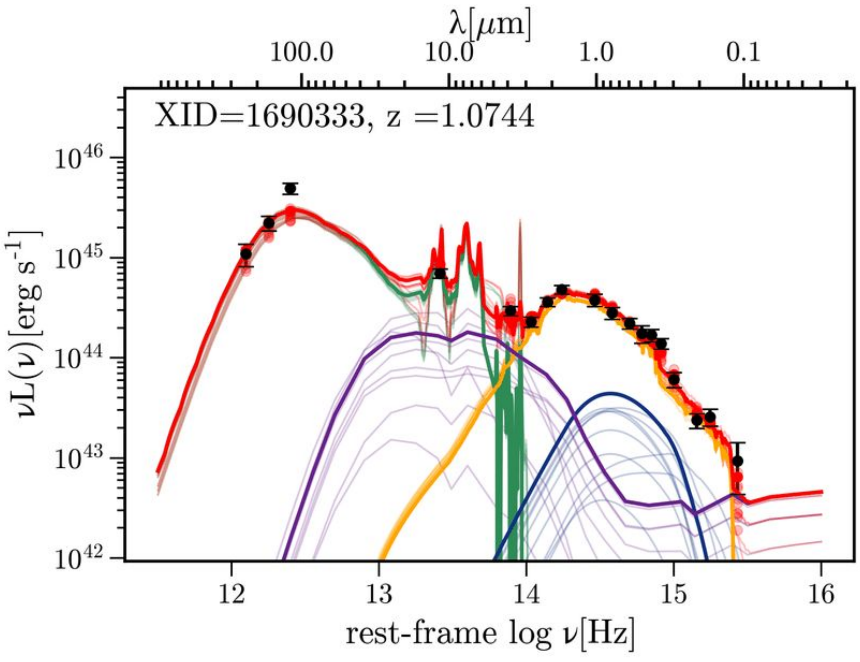

Methodology

Source selection

Result of the source selection process.

4FGL Name	RAJ2000	DEJ2000	z	TS	FOM
J0132.7−0804	23.183	-8.074	0.148	88	0.8
J0212.2−0219	33.066	-2.319	0.250	61	0.8
J0350.4−5144	57.613	-51.743	0.32h	98	0.8
J0515.5−0125	78.891	-1.419	0.25h	55	0.8
J0526.7−1519	81.692	-15.321	0.21h	218	1.6
J0529.1+0935	82.297	9.597	0.30h	86	1.3
J0557.3−0615	89.344	-6.265	0.29h	53	1.6
J0606.5−4730	91.642	-47.504	0.030	137	1.0
J0647.0−5138	101.773	-51.638	0.22h	81	2.5
J0733.4+5152	113.362	51.880	0.065	162	2.5
J0847.0−2336	131.757	-23.614	0.059	921	0.8
J0953.4−7659	148.367	-76.993	0.25h	104	0.8
J0958.1−6753	149.534	-67.894	0.21h	29	1.0
J1132.2−4736	173.056	-47.613	0.21h	129	1.0
J1447.0−2657	221.765	-26.962	0.32h	46	2.0
J1714.0−2029	258.522	-20.486	0.09h	110	2.0
J1824.5+4311	276.126	43.196	0.487	99	0.8
J1934.3−2419	293.582	-24.326	0.23h	63	1.6
J1944.4−4523	296.101	-45.393	0.21h	164	1.0
J2001.9−5737	300.491	-57.631	0.26h	123	0.8
J2142.4+3659	325.602	36.986	0.24h	110	1.3
J2246.7−5207	341.682	-52.126	0.098	95	2.5
J2251.7−3208	342.944	-32.140	0.246	52	2.0

Methodology

A note on broadband spectral modeling

fitting … seems easy

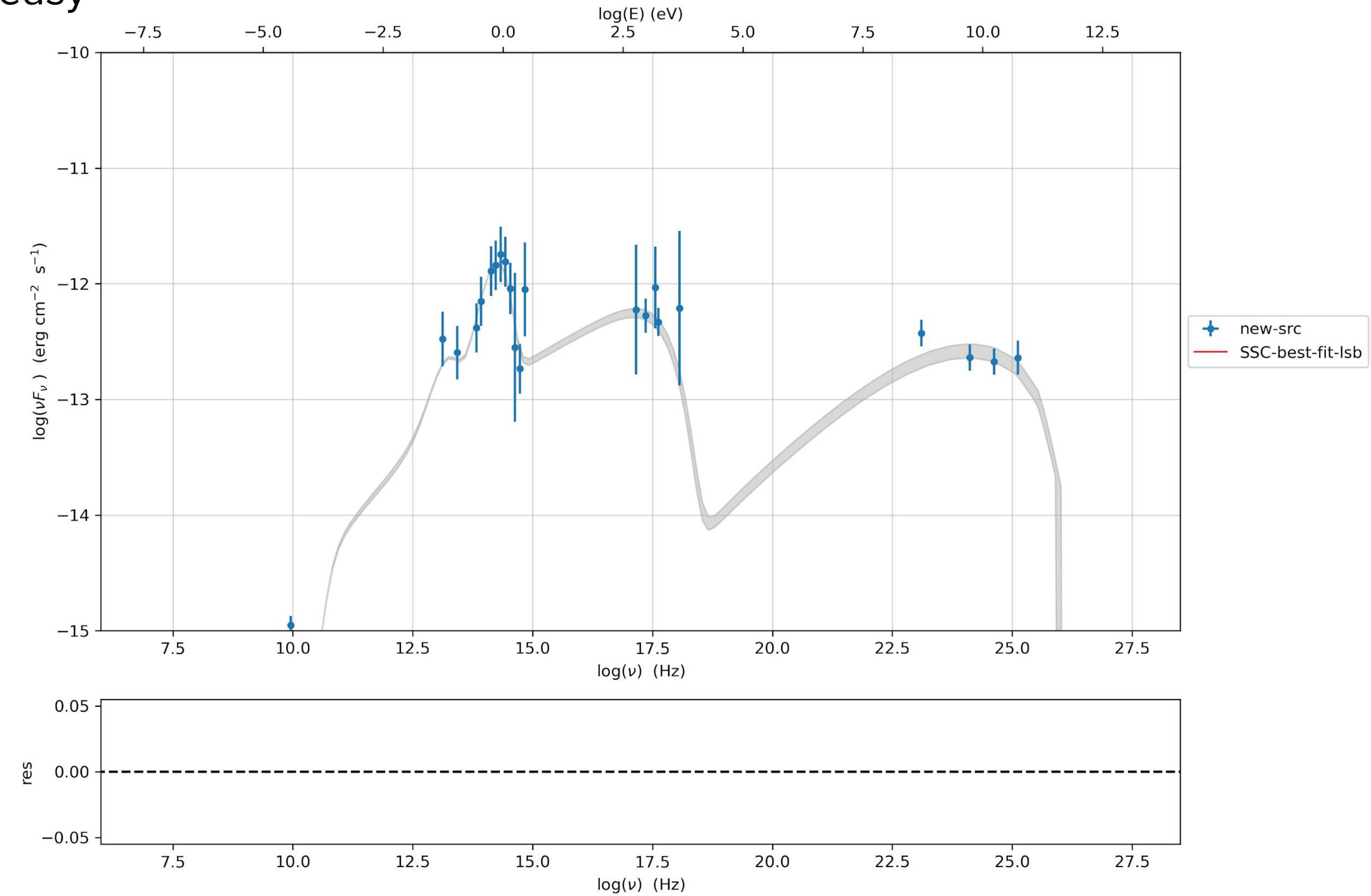

Methodology

A note on broadband spectral modeling

… but it is not

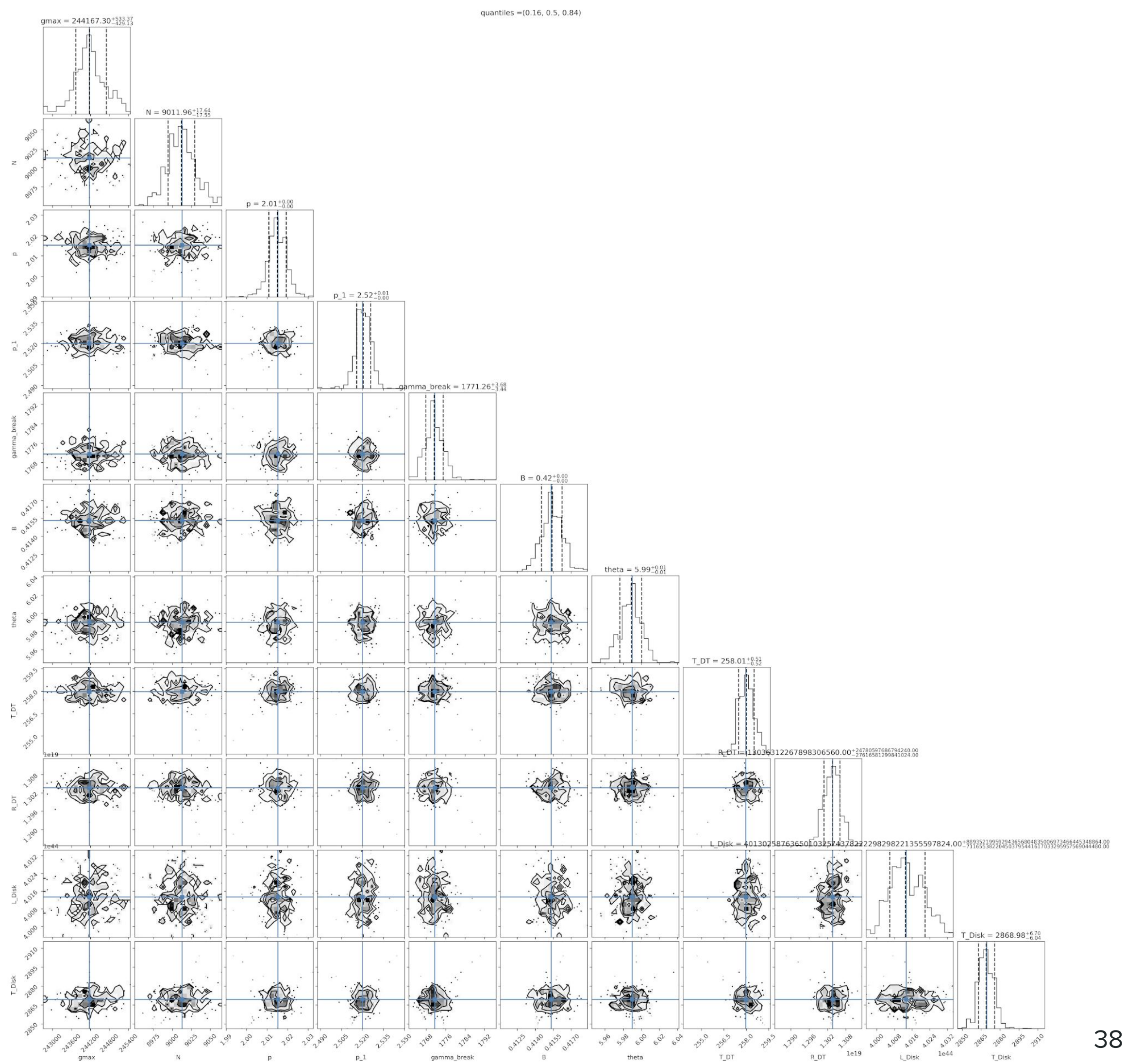

Many parameters

Lots of degeneracy

‘supervised fitting’.